BILINGUAL PUBLISHING CO.
Pioneer of Global Academics Since 1984

Non-Metallic Material Science

Volume 4 • Issue 1 • April 2022 ISSN 2661-3301(Online)

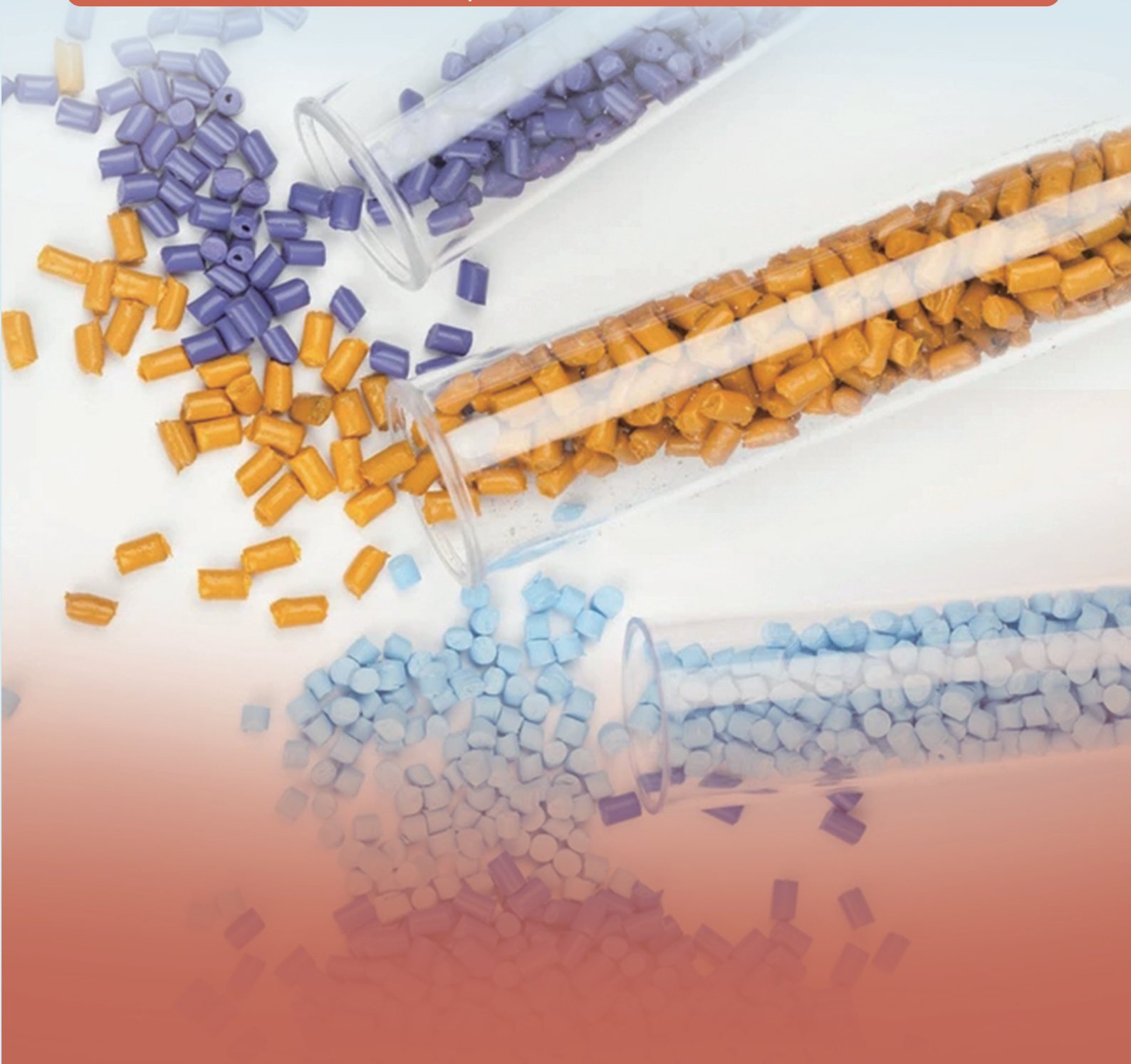

BILINGUAL PUBLISHING CO.
Pioneer of Global Academics Since 1984

Volume 4 Issue 1 · April 2022 · ISSN 2661-3301 (Online)

Non-Metallic Material Science

BILINGUAL PUBLISHING CO.
Pioneer of Global Academics Since 1984

BILINGUAL PUBLISHING CO.
Pioneer of Global Academics Since 1984

Volume 4 | Issue 1 | April 2022 | Page1-32
Non-Metallic Material Science

Contents

Editorial

Articles

Review

BILINGUAL PUBLISHING CO.
Pioneer of Global Academics Since 1984

Non-Metallic Material Science
https://ojs.bilpublishing.com/index.php/nmms

EDITORIAL

GHG Emissions and Role of Polymeric Materials in Mitigation

Muhammad Imran Rashid[1,2,3*]

1. Department of Chemical, Polymer and Composite Materials Engineering, University of Engineering and Technology, Lahore (New Campus), 39021, Pakistan
2. Center for Energy Research and Development (CERAD), University of Engineering and Technology, Lahore (New Campus), 39021, Pakistan
3. Chemical Engineering Discipline, School of Engineering, College of Engineering, Science and Environment, University of Newcastle, Callaghan NSW 2308, Australia

ARTICLE INFO

Article history
Received: 6 December 2021
Accepted: 9 December 2021
Published Online: 20 December 2021

GHG emissions of methane (CH_4) have double, and CO_2 are close to double compared to pre-industrial levels. GHG emission mitigation is possible by avoiding their generation, or by emission mitigation technologies. CO_2 can be stored/fixed in minerals, rocks, EOR, underground formations, chemicals, and polymeric materials and many more. Polymeric materials also play role in GHG mitigation, and more focus is required on this aspect. CO_2 consumption during polymerization reactions and plasticization is required to be enhanced. This fact also supports higher polymers production and increasing capacity of polymers producing industries.

Greenhouse gas emissions escalade/broke out/sparked in modern era especially CO_2 peaks at 414 ppm (2021) from 280 ppm (1750) (going to double Soon) and caused recent extreme weather patterns, threatening flooding, heat waves, glaciers lakes melting, extended summer, extreme temperatures (54 °C middle east) [1], droughts, descending water levels, oceans pollution and fresh and wastewater pH variation are warning signs of GHG emissions and anthropogenic CO_2 emissions. There are many Climate change mitigation technologies [1], however, steps/actions

*Corresponding Author:
Muhammad Imran Rashid,
Department of Chemical, Polymer and Composite Materials Engineering, University of Engineering and Technology, Lahore (New Campus), 39021, Pakistan; Center for Energy Research and Development (CERAD), University of Engineering and Technology, Lahore (New Campus), 39021, Pakistan; Chemical Engineering Discipline, School of Engineering, College of Engineering, Science and Environment, University of Newcastle, Callaghan NSW 2308, Australia;
Email: muhammadimran_rashid@yahoo.com

DOI: https://doi.org/10.30564/nmms.v4i1.4176

need to be taken at individual level. Recently, "Green Campus Initiative" is taken at UET (New Campus) where all barren land is converted into greenery by planting multiple crops. Other universities and institutes have implemented GHG emissions analyses and release estimation [2]. However, GHG and especially CO_2 is released significantly when remains of crops are burned. Particulate matter and dust from these burnings and mist, fog and smog generated rise more environmental concerns. These remains of crops may be cut into pieces instead of burning to avoid emissions. Individual initiatives may be saving trees by hard paper free environment and minimum printing i.e. "Save Trees". Coal burning must be abandoned as it significantly releases CO_2, SO_3, SO_2, NO_3 and NO_2. Similarly, there are significant emissions from brick kilns which must be mitigated using amine solutions. Transportation and forest fires also emit CO_2. In Cop26 conference, delegates from almost 200 countries participated and focus is to limit global warming to 1.5 °C as already temperatures are above 1.1 °C compared to pre-industrial values [3]. Clean energy and renewable energy resources such as hydrogen energy, solar energy, biofuels (e.g. biodiesel), wind energy, biogas, hydro energy, tidal energy, fuel cells, biomass, ocean energy and nuclear energy have become necessity to protect environment. These clean energy resources utilization will avoid harsh stance in GHG emission mitigation technologies also limiting safety concerns on geological storage, EOR, oceanic storage and others. Polymeric materials also play a role in GHG mitigation by consumption of these gases (CO_2). Polymeric and nonpolymeric sorbents (absorbents and adsorbents) are currently employed for CO_2 capture [4]. Organic polymers can store carbon dioxide [5]. These polymeric materials have high CO_2 storage capability and were thermally stable and have more pores. Polymer 5 among 4,5 and 6 showed the highest CO_2 adsorption capacity, surface area, and pore volume [5]. Telmisartan organotin (IV) containing small mesopores are also being used as CO_2 capture media [6]. Dibutyltin (IV) complex (4) was most efficient (7.1 wt% CO_2 uptake) having high surface area and volume. Among 3 polyphosphates, meta phosphate showed 6 wt% CO_2 uptake compared to minimum 4.4 wt% requirement [7]. Polymer 5 showed 14 wt% CO_2 uptake [8]. Schiff base 1 having nitro group has shown 10 wt% CO_2 uptake [9]. PIMs, COFs, PPNs, HCPs, CMPs, PAFs and CTF are modern porous materials for CO_2 Capture [4]. Further research on Schiff bases (especially melamine and nitro groups incorporation), ionic liquids/NOHMs coupling with porous organic polymers (including meta phosphate, benzidine) and activated carbons and MOFs will be key to develop more efficient materials complexes for carbon dioxide storage.

References

[1] M.I. Rashid, 2021. Truth and False-Carbon Dioxide Mitigation Technologies. Non Metallic Material Science. 3(2) 1-5.
DOI: https://doi.org/10.30564/nmms.v3i2.3724.

[2] P.Yañez, A. Sinha, M. Vásquez, 2020. Carbon Footprint Estimation in a University Campus: Evaluation and Insights. Sustainability. 12(1) 181.

[3] R. Mason P. Walker, F Harvey, 2021. Call for world leaders to 'banish ghosts of past' with Cop26 climate vows. The Guardian.

[4] A. Sattari, A. Ramazani, H. Aghahosseini, M.K. Aroua, 2021. The application of polymer containing materials in CO_2 capturing via absorption and adsorption methods. Journal of CO_2 Utilization. (48) 101526.
DOI: https://doi.org/10.1016/j.jcou.2021.101526.

[5] H.M. Safaa, A.S. Hameed, E. Yousif, M.H. Alotaibi, D.S. Ahmed, G.A. El-Hiti, 2020. New Porous Silicon-Containing Organic Polymers: Synthesis and Carbon Dioxide Uptake. Processes 8(11) 1488.

[6] A.G. Hadi, K. Jawad, E. Yousif, G.A. El-Hiti, M.H. Alotaibi, D.S. Ahmed, 2019. Synthesis of Telmisartan Organotin(IV) Complexes and their use as Carbon Dioxide Capture Media. Molecules. 24(8):1631.

[7] H.A. Satar, A.A. Ahmed, E. Yousif, D.S. Ahmed, M.F..Alotibi, G.A. El-Hiti, 2019. Synthesis of Novel Heteroatom-Doped Porous-Organic Polymers as Environmentally Efficient Media for Carbon Dioxide Storage. Applied Sciences. 9(20) 4314.

[8] D.S. Ahmed, G.A. El-Hiti, E. Yousif, A.S. Hameed, M. Abdalla, 2017. New Eco-Friendly Phosphorus Organic Polymers as Gas Storage Media. Polymers. 9(8) 336.

[9] R.M. Omer, E.T.B. Al-Tikrity, G.A. El-Hiti, M.F. Alotibi, D.S. Ahmed, E.Yousif, 2020. Porous Aromatic Melamine Schiff Bases as Highly Efficient Media for Carbon Dioxide Storage. Processes. 8(1) 17.

BILINGUAL PUBLISHING CO.
Pioneer of Global Academics Since 1984

Non-Metallic Material Science
https://ojs.bilpublishing.com/index.php/nmms

ARTICLE

Electrical Resistivity Survey on Two Waste Dumpsites at Nguru, Potiskum, Yobe State, Nigeria to Determine the Effect of Leachates on Ground Water Aquifer

G.A. Bala[1] I.G. Buba[1] S.M. Ngaram[1] O.O. Galadima[1] U. Rilwan[2*]

1. Federal University, Gashua, Yobe State, Nigeria
2. Nigerian Army University, Biu, Borno State, Nigeria

ARTICLE INFO

Article history
Received: 24 May 2022
Accepted: 30 May 2022
Published Online: 6 June 2022

Keywords:
Dumpsite
Profile
Resistivity
Leachate
Groundwater contamination

ABSTRACT

The research intends to bring out the contribution of leachate on groundwater in two dumpsites in Nguru and Potiskum all in Yobe state, Nigeria. A total of seven (7) and eight (8) VES by Schlumberger electrode with the use of Wenner electrode configuration. The results were interpreted by the use of WinRESIST for VES and IPWIN2INV for ERT. The study pointed out that, the area in question is comprised of four layers of geoelectric such as the topsoil, clay, sand, sandy clay and sand. The range of the first resistivity layer was from 6.16 Ωm to 332 Ωm in the first geo-electric layer and its thickness range from 2.77 m to 37.7 m and a depth range of 2.77 m to 37.7 m. the range of the second resistivity layer was from 16.5 Ωm to 37.9 Ωm which has the range of its thickness from 4.1 m to 10.7 m. The range of the third resistivity layer was from 101.2 Ωm to 288.2 Ωm which has the range of its thickness from 38.9 m to 99.7 m, and the first aquifer in the area. The range of the first resistivity layer was from 100.7 Ωm to 214.3 Ωm which has the range of its thickness from 28.5 m to 94 m. The fifth layer which is the second aquifer and has resistivity from 254 Ωm to 350 Ωm with a very large thickness. The range of the first resistivity aquifer is from 101.2 Ωm to 288.2 Ωm and the range of the second resistivity aquifer is from 253.8 Ωm to 350.1 Ωm. The 2D ERT profiles unveiled areas with low resistant zones and later discussed as zones penetrated by contaminants originated from dumpsites whereas high resistant zones represent areas of low or non-conductive materials in the area. Data obtained from four dumpsites indicated that leachate of the waste dumpsites penetrated into aquifers and polluted the groundwater. The existence of contaminants in the water was noted by a decrease in the formation resistant values. It is seen, from the results of the survey (geophysical) that the water in the area is polluted and it accounts for the prevalence of any disease related to water that are common in the area.

*Corresponding Author:
U. Rilwan,
Nigerian Army University, Biu, Borno State, Nigeria;
Email: rilwan.usman@naub.edu.ng

DOI: https://doi.org/10.30564/nmmn.v4i1.4740

1. Introduction

Ground water resources have been under rapidly increasing stress in large parts of the world as a result of pollution. Pollution is primarily the result of irrigated agriculture, industrialization, and urbanization, which generates large wastes, with the large impact on the ecosystem and groundwater [1]. Waste is accumulated universally and is a direct consequence of all human activities. They are generally classified into solid, liquid and gaseous.

Most human activities revolve round ground water, and its quality in a long way affects health and the socio-economic development. Anthropogenic factors contribute highly to contamination of both surface and under ground water [2]. Water contaminants have been mainly biological and chemical in origin [2,3]. The quality of under ground water could be compromised if it is not distant from constant source of pollution. Like many towns in Nigeria, Nguru and Potiskum are faced with the problems of improper collection, handling and disposal of domestic wastes. The number of man's activities has results to increase in volume of solid waste worldwide even though the current level of technological advancement and industrialization. Large growth in the population happened to be one of the major causing factors which resulted in the increase in the municipal solid waste (MSW). Filling of Land with the municipal solid waste is the most common waste management practice and one of the cheapest methods for organized waste management in many parts of the world [4-7]. In most of the low to medium income developing countries, almost 100 per cent of municipal solid waste which are accumulated goes to landfills.

Landfill operations are most feasible in these countries as land is vastly available and moderately inexpensive. Even in many developed countries where land is scarce and where policies of reduction, reuse and diversion from landfills are strongly promoted, great percentage of their accumulated municipal solid waste are still land filled. For instance, in 2006, out of the 251 million tons of MSW generated in the United States of America, 138.2 million tons representing 55% was disposed of in landfills [8]. In England, out of the 29.1 million tons of municipal solid waste generated between 2003 and 2004, 72% was land filled [9]. The scenario is similar in Northern Ireland and Scotland where 82.9% and 85.4% of their generated MSW were land filled in 2005 and 2007 respectively [10,11]. Nowadays, however, there is a successive decrease in the volume of municipal solid waste being land filled in these developed countries on a yearly basis as great efforts in solid waste management are nowadays directed towards waste reduction and recycling programmes which happened to be the real giant step in improving the environmental management [12,13]. Disposal of the refuse occurs all over the world and proves to be a major problem. Careless dumping of refuse and poor management can greatly affect one's health. Pollution from solid wastes always begins with precipitates carrying the leachates into land surface and ends with the water reaching surface water or groundwater. Precipitate on the refuse dumpsite will either infiltrate the refuse or run off over as land flow. During the vertical percolation process (with rain water) the water leaches both organic and inorganic constituents from refuse. Leachates is a fluid that results when water passes through dumpsite fraught with organic matter. It consists of water- and water-soluble compounds in the refuse that accumulate in the dumpsite as water moves through the dumpsite and its harmful contaminants pollute the underlying aquifers [14,15]. Once leachates are formed and release to ground water environment, it will migrate downward through the unsaturated zones until it reaches the saturated zone, the leachates becomes part of the ground water flow system immediately they reach the water table. The extent of pollution is greater in high rainfall areas than less humid and arid areas. Permeable soil permits rapid movement of leachates unlike in less permeable zone.

This study will unveil the effect of leachates on ground water aquifer in two waste dumpsites at Nguru, Potiskum, Yobe State, Nigeria.

2. Materials and Method

2.1 Materials

The materials used for this study of Electrical Resistivity Survey on Two Waste Dumpsites at Nguru, Potiskum, Yobe State, Nigeria to Determine the Effect of Leachates on Ground Water Aquifer are:

i. The Abem Terametre (SAS 1000).
ii. Global Positioning System.
iii. Surface 9.0 golden software package.
iv. 3D field pro software.
v. The WinRESIST version 1.0 software.

2.1.1 Geology and Location of the Study Area

The two dumpsites are located within Nguru and Potiskum L.G.A of Yobe state. They both fall within the western fringes of the Chad Basin and has some rocks of the chad formation underlying it. The Chad Basin is the largest area of inland drainage in Africa [16] occupying about 230000 kilometres-square in the central Sahara and the southern Sudan.

About one-tenth of the basin is situated in the northern part of Nigeria. The stratigraphy and composition of the

various formations are discussed [17]. Chad formation is a sequence of lacustrine and fluviatile deposits of clays and sands of Pleistocene age. These sedimentary rocks dip gently and thicken eastward towards the centre of the chad basin [18]. The chad formation consists of three water bearing horizon namely: the upper, the middle and the lower zone [18]. The upper zone provides water for numerous dug wells throughout the rural areas.

2.1.2 Nguru Dumpsite

Nguru or N'Gourou is a local government area in Yobe State, Nigeria. Its headquarters are in the town of Nguru near the Hadejia River at 12° 52' 45"N 10° 27' 09"E. It has an area of 916 km^2 and a population of 150,632 at the 2006 census.

The town probably dates around the 15th century. There is a variety of landscape types in their area, including the protected Hadejia-Nguru wetlands of Nguru Lake and the sand dunes a semi-desert area. The primary occupation of the people is farming and fishing. It also has an old wind mill company.

The dumpsite is located in an area called Hausari Sabonfegi a densely populated area in Nguru town. The post office of the town is just some few meters away from the dumpsite with a cinema viewing centre around it too. Figure 1 shows the google earth image of showing the VES line around the Nguru dumpsite.

2.1.3 Potiskum Dumsite

Potiskum or Pataskum is a local government area in Yobestae. Its headquarters is in Potiskum. It falls at 11°72' 55"N and 10°72'45". It has an area of 106 km^2 and a population of 240,547 at the 2006 census.

The dumpsite is located at the New Jerusalem settlement in Potiskum. An area where much of the churches in the town are located. Figure 2 shows image sight of the Nguru dumpsite.

2.2 Method

2.2.1 VES Data

Electrical resistivity method is an active and surface based geophysical survey method that employs measurements of electrical potential associated with subsurface electrical current flow generated by a direct current (dc) or slowly varying alternating current (ac) source and the resulting resistances are measured at the surface [19,20]. To determine the subsurface resistivity distribution, measurements are made on the surface.

These measurements involved the measuring of electrical potential associated with the subsurface electric current flow. The transmitting and the receiving electrodes are current and potential electrodes respectively.

Figure 1. Google Earth Image of Showing the VES Line Around the Nguru Dumpsite.

Figure 2. Image Sight of the Nguru Dumpsite.

2.2.2 Method of Data Collection

A total of twelve (12) electrical resistivity imaging traverse were measured in each of the dumpsites using the Wenner Array configuration with the aid of Abem Terametre. The electrode spacing for each traverse will range from 5 m to 25 m with a station interval of 5 m.

All the traverses run in the N-S direction of each dumpsites with the exception of traverses 11and 12. Traverse 1-10 of the 2D resistivity survey was mapped out within the dumpsite while the control traverses were carried out at 300 m away from each of the dumpsites. In this survey, the parameter was set for four cycle-stacking and a standard error of measurement of 5%. The recorded resistance was then be used to compute apparent resistivity values. The computer modelling was done using the WinResist software, where the calculated apparent resistivity values were processed that would yield a set of geoelectric curves, from the curves, the values of resistivity, thickness and depth of each geoelectric layer were obtained. This was constrained by a borehole lithologic log.

3. Result Presentation and Discussion

3.1 Results Presentation

The data presented in Tables 1 and 2 were used to obtained the interpretations as presented in Figures 1-13.

Table 1. Summarised result from the Nguru geo-electric from the curve profiles.

VES Location	Layer	Resistivity (Ωm)	Thickness (m)	Depth (m)	Layer Characteristics
Nguru 1	1	6.16	343	3.43	Topsoil/fine grain dry sand
	2	23.4	12.2	15.6	Laterite
	3	106	15	30.6	Shallow aquifer with Saturated coarse grain sand
	4	323			Aquifer with Saturated coarse grain sand
					Consolidated sand
Nguru 2	1	39.81	3.325	3.325	Topsoil/fine grain dry sand
	2	28.9	3.325	12.94	Laterite
	3	37.49	13.02	31	Shallow aquifer with Saturated coarse grain sand
	4	78.64			Aquifer with Saturated coarse grain sand
					Consolidated sand
Nguru 3	1	43.48	3.325	3.325	Topsoil/fine grain dry sand
	2	15.69	9.649	12.97	Laterite
	3	27.21	18.02	31	Shallow aquifer with Saturated coarse grain sand
	4	49.62			Aquifer with Saturated coarse grain sand
					Consolidated sand
Nguru 4	1	23.7	5.31	5.31	Clay sand
	2	19.3	6.93	12.2	Aquifer with saturated grain sand
	3	14.2	20.5	32.7	Consolidated sand
	4	127			
Nguru 5	1	37.3	2.77	2.77	Clay sand
	2	23.9	8.7	11.47	Aquifer with saturated grain sand
	3	41.9	25.4	36.87	Consolidated sand
	4	59			
Nguru 6	1	59.7	3.95	3.95	Clay sand
	2	31.4	11	14.95	Aquifer with saturated grain sand
	3	16	15.1	30.5	Consolidated sand
	4	59			
Nguru 7	1	52.6	4.69	4.69	Clay sand
	2	27.7	10.3	14.4	Aquifer with saturated grain sand
	3	13.6	37.7	37.7	Consolidated sand
	4	53.3			

Table 2. Summarised result from the Potiskum geo-electric from the curve profiles

VES Location	Layer	Resistivity (Ωm)	Thickness (m)	Depth (m)	Layer Characteristics
Potiskum 1	1	30.2	3.5	3.5	Clay sand
	2	77.4	1.88	5.38	Lateritic sand
	3	318	28.7	34.08	Clay sand
	4	111			Aquifer with saturated coarse grain sand
					Consolidated sand
Potiskum 2	1	56	2.57	2.57	Clay sand
	2	108	2.96	5.53	Lateritic sand
	3	395	34	3.96	Aquifer with saturated coarse grain sand
	4	167			Consolidated sand
Potiskum 3	1	26.4	3.59	3.59	Clay sand
	2	42.2	3.74	7.33	Lateritic sand
	3	286	4.1	48.3	Clay sand
	4	126			Aquifer with saturated coarse grain sand
					Consolidated sand
Potiskum 4	1	107	2.86	2.86	Clay sand
	2	31	5.65	8.51	Lateritic sand
	3	118	26.5	35	Clay sand
	4	417			Aquifer with saturated coarse grain sand
					Consolidated sand
Potiskum 5	1	65.4	1.36	1.36	Clay sand
	2	23.2	4.55	5.91	Lateritic sand
	3	298	24.3	30.2	Clay sand
	4	207			Aquifer with saturated coarse grain sand
					Consolidated sand
Potiskum 6	1	34.1	3.45	3.45	Clay sand
	2	168	26.3	29.75	Lateritic sand
	3	116	17.9	47.63	Clay sand
	4	224.3			Aquifer with saturated coarse grain sand
					Consolidated sand
Potiskum 7	1	20.8	2.86	2.86	Clay sand
	2	92.2	9.71	12.6	Lateritic sand
	3	440	16	28.6	Clay sand
	4	196			Aquifer with saturated coarse grain sand
					Consolidated sand

3.1.1 Data Interpretation

Leachate from the dumpsite was noted as a big threat to the quality of water in the area. They gradually percolate into the subsurface through the vadose zone and transfer to the aquifers where they contaminate the water. The existence of the contaminants in water was noed by a decrease in the formation resistant values. The range of low resistive zones (deep blue) was from 8 Ωm to 17.5 Ωm and explained as leachate contaminants containing toxic substances.

3.1.2 Result from the Pseudo-Profiles

From the pseudo-profiles produce from the analysis using IPWIN2 software the NW-SE pseudo-profile VES point across points 7, 1, 3 and 4, the resistivity value ranges from 8.86 Ωm to 88.6 Ωm. The dark spot points in the profiles represents regions with very low resistivity value and they are at shallow points of 1 m-4 m.

For the NS-SE pseudo-profile across VES points 6, 1, 3, and 4. Resistivity value ranges 9.41 Ωm to 94.1 Ωm.

For the SW-NE pseudo-profile across VES points 5, 3, and 2, the resistivity value ranges from 16.4 Ωm to 63.1 Ωm.

And lastly for the NNW-SSE pseudo-profile across VES points 7 and 5 with resistivity value range from 17.8 Ωm to 64.9 Ωm. The regions with the low resistivity value are at depths of 37 m-51 m. (very deep).

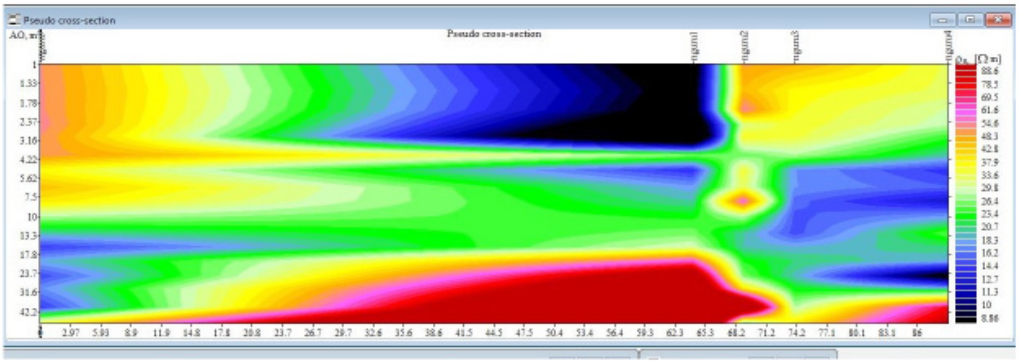

Figure 3. NW-SE Profile across VES Points 1, 3, 4 and 7.

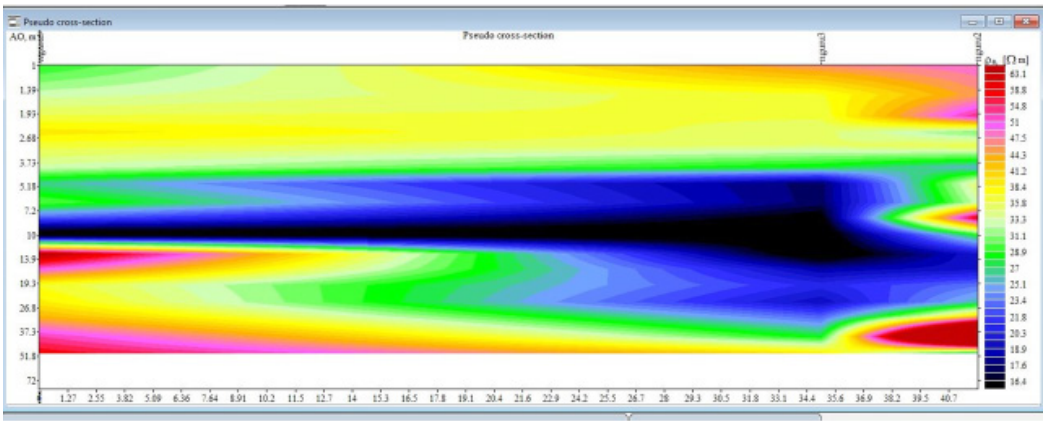

Figure 4. NW-SE Profile across VES Points 2, 3 and 5.

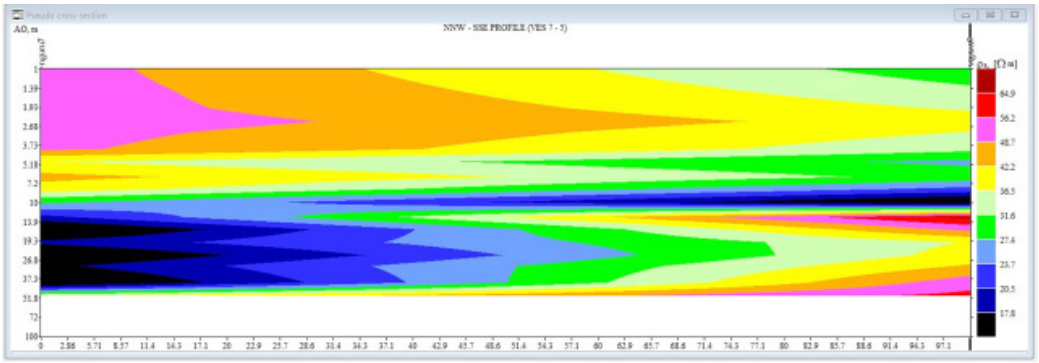

Figure 5. NW-SE Profile across VES Points 5 and 7.

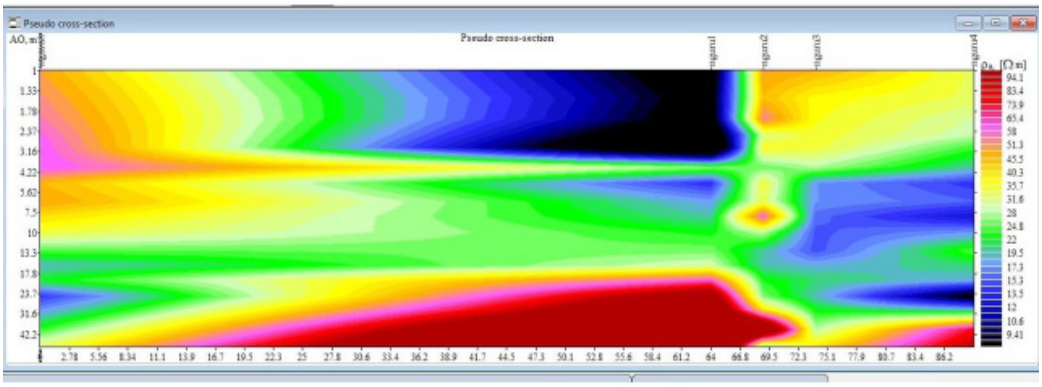

Figure 6. NW-SE Profile across VES Points 1, 3, 4 and 6.

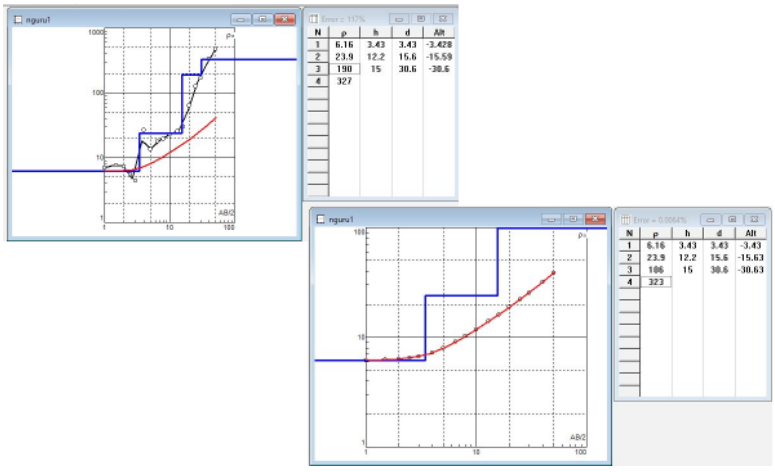

Figure 7. Geo-electric Layer curve Model for Nguru 1.

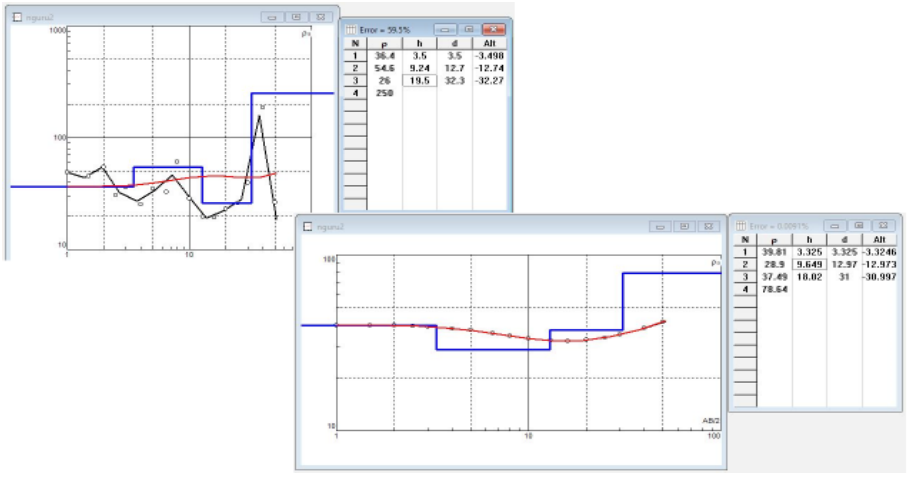

Figure 8. Geo-electric Layer curve Model for Nguru 2.

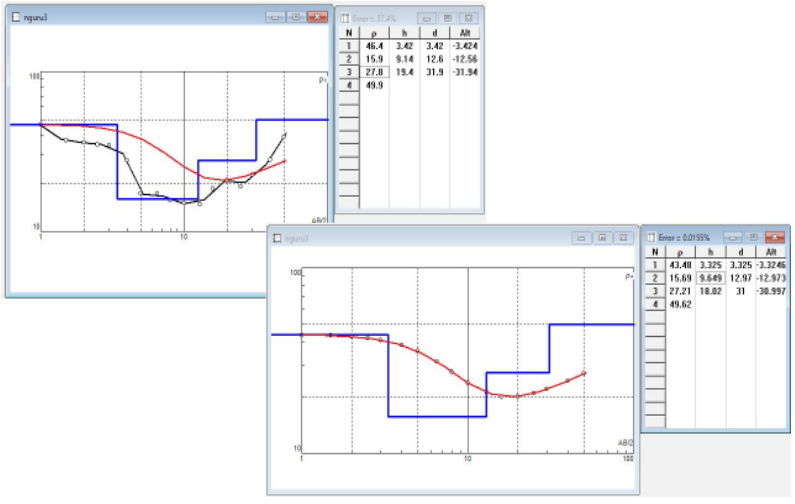

Figure 9. Geo-electric Layer curve Model for Nguru 3.

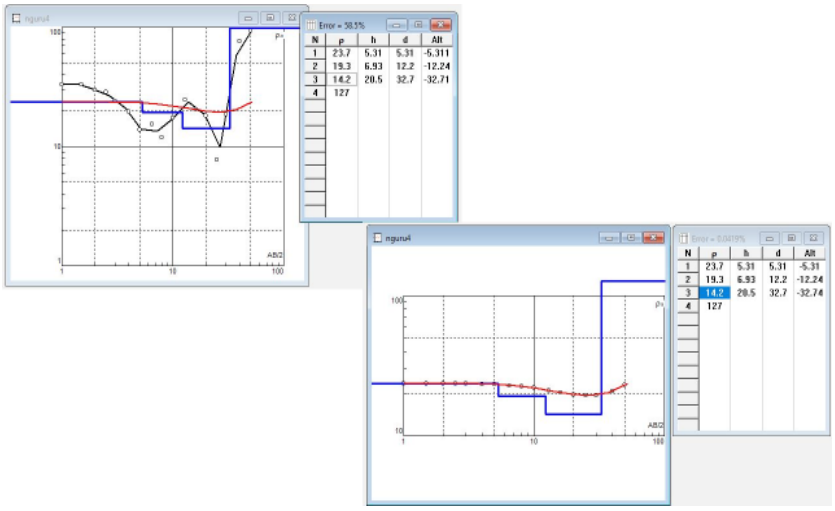

Figure 10. Geo-electric Layer curve Model for Nguru 4.

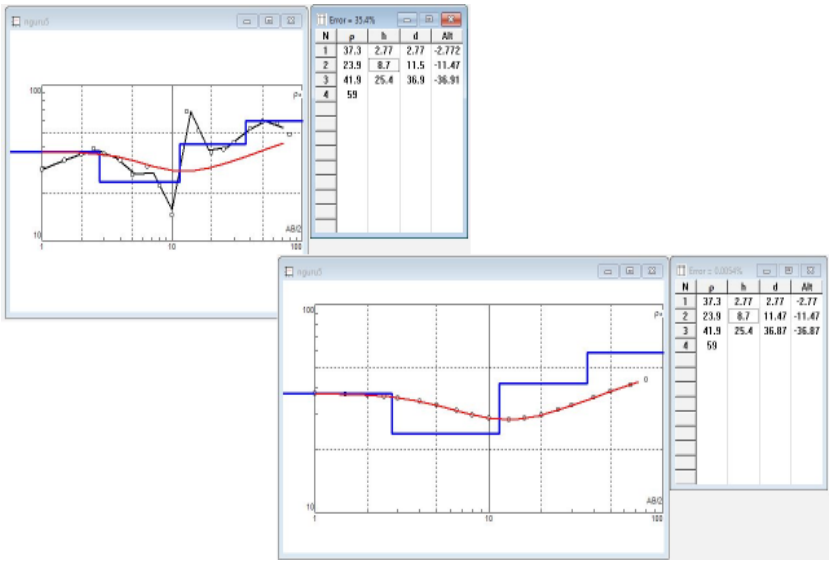

Figure 11. Geo-electric Layer curve Model for Nguru 5.

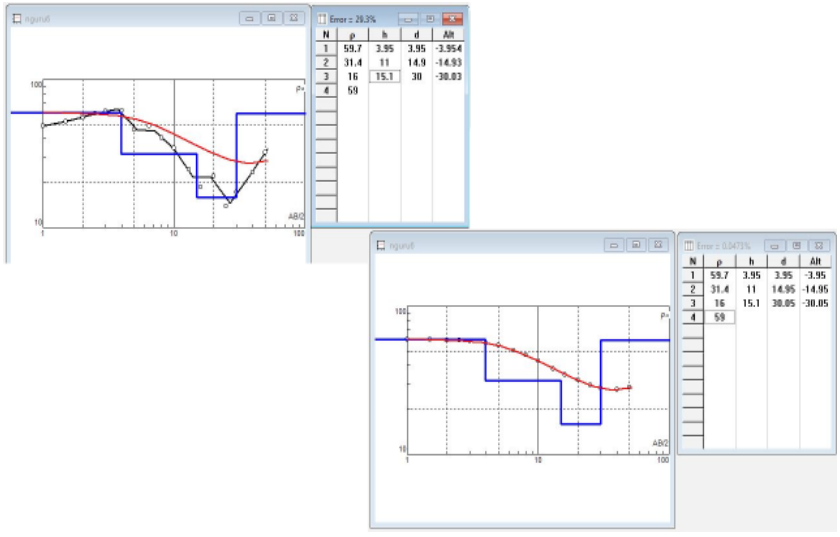

Figure 12. Geo-electric Layer curve Model for Nguru 6.

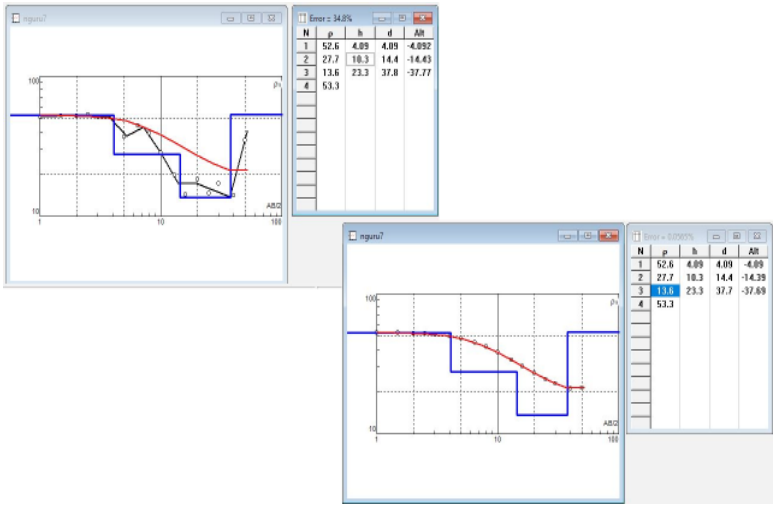

Figure 13. Geo-electric Layer curve Model for Nguru 7.

3.2 Discussion

Figures 7 to 13 show the Geoelectric sections for Nguru VES 1-7 throughout the four dumpsites of the solid waste in the area. To larger extent, the data indicate good correspondence in comparison of layers with the borehole log that exist in the location. The VES data were presented as the resist graph/VES curves (Figures 7-13). Several computations were made to ensure low root mean square (RMS) and accuracy of the data. The data of the VES helped to characterize the subsurface geology of the dumpsites.

The geo-electric layers representation was characterized as (4) four layers (Table 1) for all the (7) VES points, which are; the topsoil, clay, sand, sandy-clay and sand. For Nguru 1 geo-electric layers with four layers, the first layer has a resistivity value of 6.16 Ωm at a depth of 3.43 m, the second layer has a resistivity value 23.4 Ωm at depth of 15.6 m and lastly the third layer has a resistivity of 106 Ωm at a depth of 30.6 m. This geo-electric curve for Nguru 1 clearly shows that the resistivity value increases with depth.

For Nguru 2 geo-electric layers with four layers, the first layer has a resistivity value of 39.81 Ωm at a depth of 3.325 m, the second layer has a resistivity value 28.9 Ωm at depth of 3.325 m and lastly the third layer has a resistivity of 37.4 Ωm at a depth of 31 m. This geo-electric curve for Nguru 2 clearly shows that the resistivity value is low at the second layer which could indicate the presence of good water.

For Nguru 3 geo-electric layers with four layers, the first layer has a resistivity value of 43.48 Ωm at a depth of 3.325 m, the second layer has a resistivity value 15.69 Ωm at depth of 12.97 m and lastly the third layer has a resistivity of 27.21 Ωm at a depth of 31 m. This geo-electric curve for Nguru 3 clearly shows that the resistivity value is low at the second layer which could indicate the presence of good water.

For Nguru 4 geo-electric layers with four layers, the first layer has a resistivity value of 23.7 Ωm at a depth of 5.31 m, the second layer has a resistivity value 19.3 Ωm at depth of 12.2 m and lastly the third layer has a resistivity of 14.2 Ωm at a depth of 32.7 m. This geo-electric curve for Nguru 4 clearly shows that the resistivity value is low at the first layer which could indicate the presence of water at shallow depth.

For Nguru 5 geo-electric layers with four layers, the first layer has a resistivity value of 37.3 Ωm at a depth of 2.77 m, the second layer has a resistivity value 23.9 Ωm at depth of 2.77 m and lastly the third layer has a resistivity of 41.9 Ωm at a depth of 36.8 m. This geo-electric curve for Nguru clearly shows that the resistivity value is low at the third layer which could indicate the presence of water at a very location.

For Nguru 6 geo-electric layers with four layers, the first layer has a resistivity value of 59.7 Ωm at a depth of 3.95 m, the second layer has a resistivity value 31.4 Ωm at depth of 14.5 m and lastly the third layer has a resistivity of 16 Ωm at a depth of 30.5 m. This geo-electric curve for Nguru 6 clearly shows that the resistivity value is very at the first layer which could indicate the presence of water at shallow depth.

And lastly, for Nguru 7 geo-electric layers with four layers, the first layer has a resistivity value of 52.6 Ωm at a depth of 4.69 m, the second layer has a resistivity value 27.7 Ωm at depth of 14.4 m and lastly the third layer has a resistivity of 13.6 Ωm at a depth of 37.7 m. This geo-electric curve for Nguru 7 clearly shows that the resistivity value is very at the first layer which could indicate the presence of water at shallow depth similar to Nguru 6 geo-electric layer.

4. Conclusions

The geophysical data obtained from the area under investigation were analyzed and the results indicated that the leachate from the dumpsites of both in Nguru and Potiskum has penetrated the sandy aquifers thereby pollutes the water in the area. Hand dug well water and drilled boreholes within contamination areas may be the cause of high danger in the water of the area under study. The depth of wells in the area under study is 20 m. Many boreholes were seen in the first aquifer which are unconfined, and this makes them sensible to pollution by leachate from the dumpsites. The 1D VES and 2D ERT data revealed that the aquifers in the area under study are contaminated by leachate from dumpsites solid waste. From the findings presented, it is recommended that deeper drilling and constant monitoring of borehole water should be encouraged, government should enforce environmental protection laws that will prohibit indiscriminate disposal of solid waste material from domestic and industries. Nonetheless, this work is to be continued for more and better understanding of the area.

Conflict of Interest

There is no conflict of interest.

References

[1] Abd El-salam, M.M., Abu-Zuid, G.I., 2015. Impact of landfill leachates on the groundwater quality: A case study in Egypt. Journal of Advanced Research. 6(4), 579-586.

[2] Adefehinti, O.A., 2001. Toxicity Testing of Stimulated Leachates of solids waste from Olusosun Landfill, Ojota, Lagos. M.Sc. Thesis, Chemistry Department, University of Ibadan, Ibadan, Nigeria. 1(1), 104-105.

[3] Adefemi, O.S., Awokunmi, E.E., 2009. The impact of municipal solid waste disposal in Ado-Ekiti metropolis, Ekiti State, Nigeria. African Journal of Environmental Science & Technology. 3(8), 186-189.

[4] Adeyemi, O., Oloyede, O.B., Oladiji, A.T., 2007. Physicochemical and microbial characteristics of leachate contaminated groundwater. Asian Journal of Biochemistry. 2(1), 343-348.

[5] Akinbiyi, R., 1992. Improving the urban environment. Africa Health. 15(1), 112-124.

[6] Akpan, A.Y., 2004. Physico-chemical studies on the pollution potential of Itu River, AkwaIbom State, Nigeria. World Journal of Gastroenterology. 5(1), 1-4.

[7] Al Sahabi, E., Rahim, S.A., Wan Zahairi, W.Y., et al., 2009. The characteristic of leachates and groundwater pollution at Municipal Solid waste landfill of Ibb City, Yemen. American journal of environmental Sciences. 5(3), 256-266.

[8] Ali, M.H., Abdel-Satar, A.M., 2005. Studies of some heavy metals in water, sediment, fish and fish diets in some fish farms in El-Fayoum province. Egyptian Journal of Aquatic Research. 31, 261-273.

[9] Allen. A.R., 2001. Containment landfills: The Myth of sustainability. Journal of Engineering Geology. 60(1), 3-19.

[10] Amidu, S.A., Olayinka, A.I., 2006. Environmental assessment of sewage disposal system using 2D electrical resistivity imaging and geochemical analysis. A case study of Ibadan, southwestern Nigeria. Environmental and Engineering Geoscience. 12(1), 261-272.

[11] Aurangabadkar, K., Swaminathan, S., Sandya, S., et al., 2001. Impact of municipal solid waste dumpsite on ground water quality at Chennai. Environmental Pollution & Control. 5(1), 41-44.

[12] Aweto, K.E., Mamah, L.I., 2014. Application of resistivity methods to groundwater protection studies in Niger Delta. International Journal of Environmental Protection. 4(3), 27-35.

[13] Bahnasawy, M., Khidr, A., Dheina, N., 2011. Assessment of heavy metal concentrations in water, plankton, and fish of Lake Manzala, Egypt. Turkish Journal of Zoology. 35(2), 271-280.

[14] Barber, W., Jones, D.G., 1958. The Geology and Hydrology of Maiduguri, Bornu Province. Geological Survey of Nigeria. (1), 5-20.

[15] Daskalopoulos, E., Badr, O., Probert., S.D., 1998. An integrated approach to municipal solid waste management. Resources Conservation & Recycling. 24(1), 33-50.

[16] David, O.M., Akinwunmi, A., Oluduro, A.O., et al., 2011. Antibiotic resistance and plasmid profile of bacterial pathogens isolated from drinking water in Ado-Ekiti, Nigeria. Journal of Microbiology. 25(1), 2339-2344.

[17] Galdima, O.O., Bala, G.A., Buba, I.G., et al., 2022. Electrical Resistivity and Physio-chemical Survey Applied to the Study of Ground Water Contamination Around an Old Cemetery in Gashua, Bade Local Government Area Yobe, State, Nigeria. Acta Scientific Clinical Case Reports. 3(6), 69-80.

[18] El – Fadel, M., Findikakis, A.N., Leckie., J.O., 1997. Environmental impact of solid waste land filling. Journal of Environmental Management. 50(1), 1-25.

[19] Griffiths. D.H., Barkers, R.D., 1993. Two-dimensional resistivity imaging and modeling of complex geology. Journal of Applied Geophysics. 29(1), 211-226.

[20] Henriet, J.P., 1976. Direct application of Dar-Zarouk parameters in groundwater survey. Geophysical Prospecting. 24(1), 52-63.

BILINGUAL PUBLISHING CO.
Pioneer of Global Academics Since 1984

Non-Metallic Material Science
https://ojs.bilpublishing.com/index.php/nmms

ARTICLE

Impedance, What It Is, How It Is Measured, and Why It Is Needed

V.K. Balkhanov*

Institute of Physical Materials Science of the Siberian Branch of the Russian Academy of Sciences, Ulan-Ude, Russia

ARTICLE INFO

Article history
Received: 18 April 2022
Accepted: 1 June 2022
Published Online: 8 June 2022

Keywords:
Impedance
MSI
Underlying medium
Logging

ABSTRACT

Impedance is the basic concept and quantity when measuring an electromagnetic field near the earth's surface. It is shown how the antennas of the IPI device are oriented, and how the coordinate system is set. It is established why the phase difference of the electromagnetic field component is limited to the limits from zero to minus ninety degrees. The introduction of the basic electrophysical characteristics of a continuous medium - dielectric constant and electrical conductivity - is considered. For a homogeneous medium, the dependence of impedance on electrophysical quantities is given. The Riccati equation for impedance is given. Not only the horizontal arrangement of the electrical cable is considered, but also the vertical one. The latter allows you to explore the electrical parameters of the media.

1. Introduction

In the theory of electromagnetism and geoprospecting, an important quantity is impedance, defined as the ratio of the components of the electric field to the magnetic field near the earth's surface. This definition introduces the Cartesian coordinate system. The importance of this value is manifested in the fact that the phase difference of the components of the electromagnetic field is exactly equal to the phase of impedance. The work will establish that the impedance phase is limited to the limits from 0 to minus ninety degrees. To deal with electromagnetic waves, the impedance must be much less than one, this is the Leonitovich-Shchukin condition. A homogeneous underlying medium has constant values of electrical conductivity and dielectric constant, which are related to impedance. The real underlying media are heterogeneous, in which the electrical conductivity and dielectric constant depend on the depth of the earth's rocks. Impedance allows you to enter effective values of electrical conductivity and dielectric constant. The Riccati equation for impedance is given. Not only the horizontal arrangement of the electrical cable is considered, but also the vertical one. The latter allows you to explore the electrical parameters of the environment. In order not to talk about geoelectrics, now we need to talk about impedance media.

*Corresponding Author:
V.K. Balkhanov,
Institute of Physical Materials Science of the Siberian Branch of the Russian Academy of Sciences, Ulan-Ude, Russia;
Email: ballar@yandex.ru

DOI: https://doi.org/10.30564/nmms.v4i1.4640

2. Electrical Conductivity, Resistivity and Dielectric Constant

First, let us recall the meaning of the basic quantities used in electromagnetism.

All continuous media consist of charged particles - electrons and nuclei, which are grouped into atoms and molecules, and are in perpetual motion. At distances much larger than the size of nuclei, all charged particles interact with each other through electric fields, which, in fact, charged particles bind together into atoms and molecules. We consider distances, much larger than the sizes of atoms and molecules, when it is necessary to take into account the laws of quantum mechanics, and it is possible not to be distracted (within the limits of our article!) by the laws of quantum mechanics.

Under the influence of an external electric field, all charges come into motion. Electrons begin to move away from atoms, molecules change their geometric shape. It is usually said that the continuous medium acquires dielectric properties. This property is described by the introduction of the dielectric constant of the substance that is denoted by how ε. The presence of dielectric properties leads to reduction of the vector of the external electric field E up to value E/ε in dielectrics.

The vector does not change direction, but decreases in magnitude, {but it is possible to create modern metamaterials that also change the direction of the vector}. It follows from this definition that the dielectric constant is a dimensionless quantity. If the dielectric constant is one (ε=1), then the external electric field does not change, remaining unchanged in magnitude and direction. Such an environment is free space - air, atmosphere and all empty space. Since all continuous media are composed of charged particles, all substances are actually **dielectrics**. This leads to the fact that the light is refracted in the glass, and is delayed by the wall, through which we do not see anything. And to many other effects that we will not dwell on.

Let's talk a little about the value of the dielectric constant. Being on the street, we easily look around the surroundings through the air. Therefore, the dielectric constant of the air medium is one (ε=1). Something is visible through a rare shrub, so its dielectric constant will be slightly greater than one (for example, equal to ε=1.1).

In some continuous media, some electrons feel free. Then any external electric field will set them in motion. We say that an electric current (usually referred to as I) has appeared in the medium. It can be easily measured with an ammeter! Media that have free electrons are called conductors. This property is described by electrical conductivity (designated, how σ). Since one part of the charged particles is attached inside the medium, and the other part in it is free, all substances can have both properties at once, i.e. dielectrics can often conduct an electric current. In this case, they can be called semiconducting (not to be confused with semiconductors! - a separate class of materials in which charges of different signs play an equal role), in which electrical parameters ε and σ play equal roles. The movement of free charges is mainly influenced by the nuclei of atoms and molecules, which inhibit the movement of charges, thereby reducing the electric current. This phenomenon is described by the introduction of specific *electrical resistanc* (denoted by how ρ). Since the ability to conduct an electric current and resist it are the flip sides of a single phenomenon, conductivity and resistivity must be related to each other. In their distant time, they were defined as inverses of each other, i.e.

$$\sigma = 1/\rho. \quad (1)$$

In different formulas, you can use both notations in the same way, just without confusing them with each other. Some researchers are accustomed to using conductivity, others - resistivity. (And, sometimes, when talking about the same thing, they don't understand each other; don't be like them!).

We do not give in the form of tables the values of the dielectric constant and conductivity of various media and materials. They are easy to find on the Internet (previously, the researcher had to have solid reference books for this, they say, when asked whether he remembers certain or constant ones, A. Einstein replied that no - he takes the necessary values from reference books). But we can't resist, and we'll give these values for the two environments. For Baikal water (the purest water in nature!):

dielectric permeability ε = 81;

specific resistance ρ =150 $\Omega \cdot m$.

For granitic rocks (the main rock that makes up the earth's crust and lithosphere):

dielectric ermeability ε = 5;

specific resistance ρ =10^6 $\Omega \cdot m$.

Thus, we demonstrate the range of these quantities.

3. Electromagnetic Field and Wave Number

Everything that is under our feet is called the underlying media. These are forest vegetation, a layer of soil, water mass and sedimentary rocks. The Earth's atmosphere is literally filled with electromagnetic fields of different nature and different frequencies. They spread differently along the earth's surface and penetrate into the underlying media. It would be a sin not to use these fields to probe the terrestrial media. In the atmosphere, electromagnetic

waves propagate in the same way as in free space. These waves have electric vectors ***E*** and magnetic ***H*** fields simultaneously reach their maximum value and also simultaneously pass through zero (Figure 1). To put it another way, the electric and magnetic fields in free space are in phase with each other.

It turns out that electromagnetic waves, regardless of frequency in empty space, always propagate at the same speed - the speed of light c (in SI $c=10^8$). Thus, the frequency (denoted by f, measured in Hz = 1/sec) becomes of fundamental importance. No wonder, all electrical appliances, if anything, measure, but always on some a certain frequency. The distance between two zero values received, for example, by an electric vector, is called the wavelength (denoted by λ, and is mwasured in m). Moreover, the wavelength, frequency and speed of light are related by a simple ratio:

$$\lambda f = c. \tag{2}$$

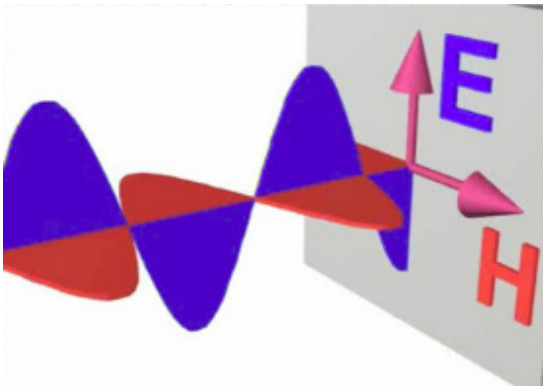

Figure 1. Electric ***E*** and magnetic ***H*** fields in free space.

Although the exact value of the speed of light in SI is known:

$$c = 2.9979\times10^8,$$

but for evaluation you can take

$$c = 3\cdot10^8\ m/s$$

(thus we make a mistake less than 0.3%). Then the electromagnetic wave with a frequency of 1 MHz will have a wavelength $c = \frac{3\cdot10^8}{10^6} = 300 \pm 1$ m/s.

If we measure an electromagnetic wave, then it means that it came to us from somewhere, i.e. had a certain direction. To indicate this direction, you entered a ***wave vector k***, the numerical value of which for a wave in free space is defined as $k = 2\pi/\lambda$. Together with the wave number, it is convenient to enter a circular frequency $\omega = 2\pi f$. Using a wave number and a circular frequency, the propagation of an electromagnetic wave along a positive direction, for example, the x-axis, will be described by the following expression:

$$\exp(ikx - i\omega t). \tag{3}$$

This expression is called a *plane wave*.

An electromagnetic wave can propagate in a continuous medium, we see through glass. Therefore, in this case you can enter a wave number k, which has an electromagnetic wave in matter. It turns out that the square of a wave number in an impedance homogeneous medium is given by the following well-known expression [1]:

$$k^2 = \frac{\omega^2}{c^2}\varepsilon + \frac{i\,\mu_0\,\omega}{\rho}. \tag{4}$$

Here in μ_0 - magnetic constant (in SI $\mu_0 = 4\pi\cdot10^{-7}$). The rest are defined above. The two terms in this expression allow environments to be divided into two classes. If in some range of frequencies in the expression (4) the first term prevails, then the medium is called capacitive. If the second term is predominant, then the medium is considered inductive (or conductive). When both terms play the same roles, then the medium will be called impedance (although previously defined as semiconducting, but the name “impedance medium” is more successful).

4. Impedance, Its Measurement and Coordinate System

Measurement of electromagnetic waves, their reception, is carried out by special equipment - SIM (surface impedance meter [2]), an integral attribute of which is an electric antenna that responds to an electric field, and a magnetic sensor in the form of a frame for measuring a magnetic field (Figure 2, Figure 3, Figure 4). The electric field is measured simply by an electrical wire isolated from contact with the ground. A magnetic sensor is a regular square frame on which another electrical wire is wound. The plane of the frame is oriented to the maximum reception of the electromagnetic signal and is taken as the y-axis. The electrical wire is orthogonal to the frame and is positioned in the direction of the signal source (usually the radio station), and this orientation is taken as the x-axis. The third axis of z coordinates is orthogonal to the x and y axes and is usually oriented from the surface of the earth into the atmosphere. Thus, a rectangular (Descartes) coordinate system was introduced.

Electromagnetic fields always have some source of their radiation, the characteristics of which are often unknown. Even if it is known that if a particular wave is emitted by a certain radio station, then the parameters of the wave at the place of its reception are strongly influenced by the presence of the earth itself. The terrain, the distribution of electrical parameters on the ground, all

this affects what wave we receive at the reception point. According to the book [3], "The medias that have to be dealt with in the theory of the propagation of radio waves along the earth are the soil and the atmosphere". And further [3], "… the surface layer of the earth always behaves completely differently with respect to waves of different frequencies". But in 1950, Academician A.N. Tikhonov pointed out that if the receiving equipment was tuned to measure not the components of the electromagnetic field themselves, but their ratio, then the parameters of the source would decrease. The resulting value of the ratio of the electric field to the magnetic field was called the surface impedance, and was designated by the symbol δ [4-6]:

$$\delta = -\frac{1}{Z_0}\left(\frac{E_x}{H_y}\right)_{z=0}. \quad (5)$$

Vacuum resistance is inyrodoced here $Z_0 = \sqrt{\mu_0/\varepsilon_0} = 376.3\,\Omega$ in order for the magnitude of the impedance to be dimensionless (therefore, it is sometimes called reduced when it is made of a dimensionless value).

The electromagnetic field equations (i.e., Maxwell's equations) are linear, so their solution can be sought in a complex form; so, temporary dependence is immediately sought in the form of $\vec{E}, \vec{B} \sim e^{-i\omega t}$. This means that impedance is a complex quantity. It is written in two forms. Or as

$$\delta = |\delta| exp(i\varphi_\delta), \quad (6)$$

where is $|\delta|$ module and φ_δ - impedance phase. Or as

$$\delta = \mathrm{Re}\,\delta + i\,\mathrm{Im}\,\delta, \quad (7)$$

where is $\mathrm{Re}\delta$ - valid and $\mathrm{Im}\delta$ - imaginary parts of the impedance.

If we combine the formulas (5) and (6), we get:

$$E_x = Z_0|\delta|H_y exp(i\delta_\varphi), \quad (8)$$

(I'm more impressed with this record). The result means that in an electromagnetic wave, the magnetic field is phase ahead of the electric field. Moreover, this phase is equal to the impedance phase.

It follows from Figure 1 that there is no phase lag in free space, i.e. in this case the phase of the impedance of free space is equal to $\delta_\varphi = 0°$. It is easy to establish that when the sine wave is shifted to $\lambda/4$ the absolute values of the fields will not change ($|E(x)| = \left|E\left(x \pm \frac{\lambda}{4}\right)\right|$). This circumstance is equivalent to the fact that the phase difference between the electric and magnetic fields will be periodic in 90°.

Figure 2. Surface impedance meter kit (MSI-300). The number 300 indicates the measuring range in kHz. A reeled insulated cable and frame are shown.

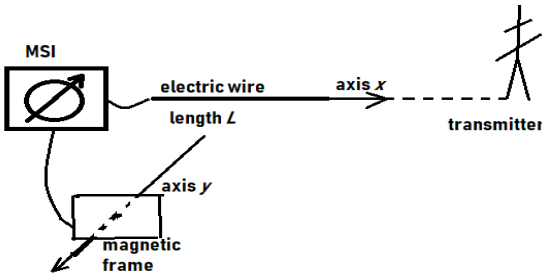

Figure 3. Surface impedance meter, orientation of electric and magnetic field meters along coordinate axes. The electric antenna lies on the ground, i.e. has a horizontal orientation.

Taking into account the sign of this phase difference, we come to the position that the phase δ_φ always extends from 0° before –90°. And this circumstance does not depend on the presence or absence of foreign bodies. The diversity of the structure of the earth's surface means that, in general, the impedance phase can have any value - from zero to zero -. Hence 90º, the difference in the phase of electric and magnetic fields in Figure 1 will be any, depending on the presence of the underlying medium, and in general, on the presence of foreign bodies.

An interesting and curious history of the appearance of the concept of impedance is given in the articles [4,5]. In short, the story goes like this. The concept of impedance was introduced into electrodynamics O. Heaviside and O. Lodge. The introduction of impedance can be traced back to electrical engineering, as S.A. Schelkunoff did back in 1938, and as detailed in Feynman's Physics Lectures. In these lectures, impedance is called complex resistance *Z*, which is the coefficient of proportionality between the voltage in the circuit *U* and the current *J*: *U* = *Z J*.

The voltage is created by the electric field E in a section of length L, so that impedance (aka complex circuit resistance) $Z = U / J = EL / J$. But the magnitude J/L is a current per unit length and determines the strength of the magnetic field H, *i.e.* $Z = E / H$. By introducing a dimensional multiplier in the form of vacuum resistance with resistance dimension, we arrive at the surface impedance given by the ratio (3).

Figure 4. Modified IPI-300 kit for measuring the electrophysical characteristics of the forest media. Vertical orientation of the electric antenna. 1. Telescopic rod; 2. Rod support; 3. Bottom mount; 4. Electric antenna suspension; 5. Dipole Nadeenko; 6. Input antenna amplifier; 7. Shielded wire; 8. Magnetic antenna; 9. MSI-300.

5. Leontovich-Shchukin Condition for Impedance

Taking the underlying medium for electromagnetic waves homogeneous, with constant values of dielectric constant and resistivity, from Maxwell's equations we can find:

$$\delta = \left\{1 + \varepsilon + \frac{i\sigma}{\varepsilon_0 \omega}\right\}^{-1/2} = \frac{1}{\sqrt{1 + \varepsilon + i/\varepsilon_0 \omega \rho}}. \quad (9)$$

Here $\varepsilon_0 \omega \rho$. all the values are already familiar to us. Let's take it as a postulate: ***the impedance task completely determines the electromagnetic fields in the air and in the underlying medium***. Although not in every case it is easy to do. Looking at the formula (9), we notice that the impedance depends on the dimensionless parameter - $\varepsilon_0 \omega \rho$. Let's evaluateit by putting the $\sqrt{-i} = (1-i)/\sqrt{2}$ frequency at 50 kHz and $\rho = 150\,\Omega \cdot m$ (typical value for Baikal water is taken):

$$8.85\times10^{-12} \times 2\pi \times 50000 \times 150 = 4\times10^{-4} << 1.$$

It turns out that for many practically important tasks of geophysics and electrical exploration, this parameter is almost always much less than one:

$$\varepsilon_0 \omega \rho \ll 1. \quad (10)$$

The smallnes of this dpmensionless parameter makes it possoble to greatly simplify both the calculation themselves and resulting formulas. So, for a homogeneous medium, in the firsr non-disappearing limit for a small parameter $\varepsilon_0 \omega \rho$, its inverse value turns out to be much-greater that one, and in any case, mire that the component $1 + \varepsilon$. Neglecting it, the impedance of (9) remains:

$$\delta = \sqrt{-i\varepsilon_0 \omega \rho}, \quad (11)$$

and for its module and phase:

$$|\delta| = \sqrt{\varepsilon_0 \omega \rho}, \ \phi_\delta = -\frac{\pi}{4} = -45^0. \quad (12)$$

In this form, the impedance (its module and phase) is usually recorded for a homogeneous conductive medium. It can be said that when propagating over a conductive medium, the electric field, in comparison with free space, lags behind the magnetic field in phase by one eighth of the complete displacement.

For compleness, we give the values of the actual and imaginary parts of the impedance in question. As $\sqrt{-i} = (1-i)/\sqrt{2}$, that

$$\mathrm{Re}\,\delta = \sqrt{\varepsilon_0 \omega \rho / 2}, \ \mathrm{Im}\,\delta = -\sqrt{\varepsilon_0 \omega \rho / 2}.$$

The imaginary part of the impedance turns out to be a negative value, and in magnitude it is equal to the actual part.

In 1938, specially for electromagnetic waves, surface impedance was introduced by M.A. Leontovich. At the save time, from (10) and (12) it turns out that electromagnetic waver the impedance modulus $|\delta|$ turns out to be noticeably less than one (don't forget that!):

$$|\delta| << 1. \quad (13)$$

This inequality will be called the Leontovich-Shchukin approximation (in 1940 Shchukin published a book [6], in which he made extensive use of impedance).

For practical purposes [7,8] it is sufficient to assume that

$$|\delta| \le 0.3. \quad (14)$$

Only in this case can we speak of electromagnetic fields as waves, variables in space and time. For example, near the emitter, the antenna is a static electric dipole. Then the magnetic field turns to zero, and the impedance (9) diverges, i.e. turns to infinity. However, in reality, electromagnetic waves can always be measured near the emitter, only they will have a bizarre spatial characteristic (the dependence of the field on the distance from the emitter). And at the same time, the Leontovich-Shchukin condition (13) will be fulfilled.

To determine the components of an electromagnetic

field, the so-called wave equations are usually derived from Maxwell's equations. They are usually solved either by separating variables or by using the Fourier-Hankel transform [9]. But if we are interested in a directly measurable quantity - impedance, then we can establish an equation for it:

$$\frac{d\delta}{dz} = \frac{i\omega}{c} + \mu_0 c\sigma(z)\delta^2. \quad (15)$$

Mathematically, this is the Riccati equation, which is usually studied in mathematical physics courses (I may discuss it in one of the next articles).

6. Determination of Electrical Parameters for Impedance Measurement

The earth's interior is highly heterogeneous. According to the basic tenets of the theory of global tectonics, the lithosphere, the outer solid surface of the Earth, is a relatively rigid shell "floating" on the surface of a very viscous mantle. The shell is divided by tectonic disturbances into large and durable lithospheric megablocks - plates, the linear dimensions of which reach several thousand kilometers. Large tectonic plates are made up of smaller structural blocks, which in turn are broken down into many even smaller blocks. The real rock mass of the Earth's lithosphere is thus a complex hierarchical tile system of blocks decreasing in size. The hierarchical structure of the surface layer of the earth will also affect the response of the electrical parameters of the system to the external electromagnetic field. When measuring the impedance, we will obtain some effective values of the electrical conductivity σ_{ef} and dielectric conductivity ε_{ef}. In 1952, to study heterogeneous media, the French researcher L. Cagniart introduced apparent resistance. The idea of introducing it is very simple. If the impedance modulus was measured $|\delta|$, then, according to the formula (9) $|\delta| = \sqrt{\varepsilon_0 \omega \rho}$, convenient to enter

$$\rho_{eff} = \frac{|\delta|^2}{\varepsilon_0 \omega}. \quad (16)$$

This is the meaning of apparent resistance that the medium would possess if it were homogeneous. It is not difficult to obtain if the impedance phase and the effective value of the dielectric constant are known. To do this, taking into account the replacement of the dielectric constant and resistivity with their effective values, we will rewrite (9) in the following form:

$$\delta^2 = \frac{1}{1 + \varepsilon_{eff} + i/\varepsilon_0 \omega \rho_{eff}} = |\delta|^2 \exp(2i\varphi_\delta)$$

Then we separate the actual and imaginary parts. The resoulting two equations are solyed with respect to $1 + \varepsilon$.

Result (17) clarifies the definition (16). Because for a homogeneous conduction media. Then we separate the actual and imaginary parts. The resulting two equations are solved with respect to $1 + \varepsilon$ and $\sigma/\varepsilon_0\omega$, then we find:

$$\rho_{eff} = \frac{|\delta|^2}{\varepsilon_0 \omega} \frac{1}{|\sin 2\varphi_\delta|}, \quad (17)$$

$$1 + \varepsilon_{eff} = \frac{\cos 2\varphi_\delta}{|\delta|^2}. \quad (18)$$

Result (17) clarifies the definition (16). Because for a homogeneous conduction media $\varphi_\delta = -45°$, then (17) goes to (16).

Similar to the introduction of effective resistivity and dielectric constant, an effective skin layer can be introduced $H_s = \sqrt{2\rho/\mu_0\omega}$ replacement ρ *on* ρ_{eff}:

$$H_s = \sqrt{\frac{2\rho_{eff}}{\mu_0 \omega}}. \quad (19)$$

We encounter this value in problems related to the heterogeneity of the media. Now, taking into account the replacement of electrical parameters with their effective values, the wave number will change, become effective:

$$\tilde{k} = k_0 \sqrt{\varepsilon_{eff} + \frac{i}{\varepsilon_0 \omega \rho_{eff}}}. \quad (20)$$

By combining impedance (4.1), only with the replacement of electrical parameters with their effective values, $\delta = \frac{1}{\sqrt{1+\varepsilon_{eff}+i/\varepsilon_0\omega\rho_{eff}}}$, with a ratio (20), find

$$\tilde{k} = k_0 \frac{\sqrt{1-\delta^2}}{\delta}. \quad (21)$$

This relation expressed the wave number in the impedance medium through the impedance itself.

It has already been mentioned above that real natural environments are heterogeneous. Just now, formulas (16) to (21) simulated inhomogeneous media with effective electrical parameters. Their dielectric and conductive properties randomly change from one location to another. This situation is often modeled with a layered medium, when in a wide range of frequencies each layer has homogeneous electrical parameters. After a homogeneous environment, the next model is a two-layer model. Then three-layer, etc. In certain frequency ranges, many terrestrial surfaces are enough to simulate with a two-layer medium. Such environments are quite widely represented on the ground. For example, ice on the water, forest on the ground, etc. So, in winter on the Northern Sea Route and on the salt lakes of Eurasia (Southern Siberia, Mongolia and China) Radio routes can be simulated as a two-layer medium, where the first medium (ice, forest) is a dielectric

layer, and the second (sea, salt water, soil) in a wide frequency range of radio waves is the underlying conductive medium. Now we can see what values of the impedances of real media correspond to the effective electrical parameters and the skin layer. We have formulas (17) to (20) for this.

Example 1. We have a radio route "ice-salt water" near the village of Tiksi, at a frequency of 10 MHz (λ_0 = 30 m), impedance was measured $\delta = 0.185\ \exp\left(-82.5^0\right)$. Now we can consistently find:

$$\rho_{eff} = 1.8 \cdot 10^7 \frac{0.185^2}{10^4 \left|\sin 165^0\right|} = 238\ \Omega \cdot m,$$

$$\varepsilon_{eff} = -1 + \frac{\cos 165^0}{0.185^2} = -29.2,$$

$$H_s = 15.9\sqrt{\frac{238}{10^4}} = 2.45\ \text{m}.$$

Example 2. Lake Sulfate: frequency 10 MHz (λ_0 =30 m), $\delta = 0.152\ \exp\left(-65.6^0\right)$,

$$\rho_{eff} = 55.3\ \Omega \cdot m,\ \varepsilon_{eff} = -29.5,\ H_s = 1.2\ m.$$

Note that the effective value of the dielectric constant for some media has not only a negative value, but also a large absolute value.

7. Impedance Measurement in Forest and Mine (Logging)

The magnetic frame is always positioned in its plane orthogonally to the direction of the radio station, as in Figures 2-4. If the electrical cable is spread on the ground, then we can calculate from the formulas (17) and (18) the electrical parameters of the underlying medium. However, the electrical cable can also be positioned vertically. Then we will be able to restore the electrical parameters of not the underlying environment, but the environment, for example, the forest layer in Figure 4.

Let's place a measuring complex in the forest [10] with vertical orientation of the electrical cable. The measured impedance, which we call normal, will be (try to get it yourself, we will do it below):

$$\delta^n = \frac{\omega\lambda}{ck^2}, \tag{22}$$

where is the square of the wave number of the forest-layer

$$k^2 = \frac{\omega^2}{c^2}\varepsilon_w + i\mu_0\ \omega\ \sigma_w. \tag{23}$$

In here σ_w and ε_w - conductivity and dielectric constant respectively of forest vegetation.

Formulas (22) and (23) can be used only for a homogeneous continuous medium, as the forest layer appears in the LW-HW ranges. Substituting $\lambda = \omega / c$ and (22) to the ratio (23), we get

$$\delta^n = \frac{1}{\varepsilon_\sim}, \tag{24}$$

where is the complex permeability

$$\varepsilon_\sim = \varepsilon_w + \frac{i}{\varepsilon_0\ \omega\ \rho_w}. \tag{25}$$

Here is the resistivity $\rho_w = 1/\sigma_w$. As $\delta = |\delta| e^{i\varphi_\delta}$ then, separating the actual and imaginary parts, from (24) and (25) we find the calculation formulas for determining ρ_w and ε_w:

$$\varepsilon_w = \frac{\cos\varphi_\delta}{|\delta|}, \rho_w = \frac{|\delta|}{\varepsilon_0 \omega \sin\varphi_\delta}. \tag{26}$$

For the first time the formula (24) was obtained by V.A. Egorov. Thus, it was established that the specific electrical resistance of the forest layer in question $\rho_w = 37 \pm 12\ k\Omega \cdot m$, and dielectric constant $\varepsilon_w = 1.6 \pm 0.3$.

Since the beginning of the last century, at the instigation of the French brothers of Schlumberger engineers, the method of VES (vertical electric sounding) has been widely used to find oil and gas fields, when electrodes are driven into the surface of the earth, and a direct or low-frequency electric current is supplied through them [11]. By measuring the electrical potential between the electrodes, it is possible to judge the electrical conductivity of the earth's depths, and already from these values to predict the presence and power of minerals. However, this ignores another useful electrical characteristic of rocks, this is their dielectric constant. The values of the dielectric constant, coupled with conductivity, can and should also characterize the presence of certain rocks in the depths of the earth's interior. As we show, for this it is necessary to use natural or artificial variable electromagnetic fields from various sources - radio stations and specialized emitters. At the same time, it is possible to use already existing measuring complexes, such as MSI, with the addition of a magnetic sensor to them - frames with wound electrical wires. The dimensions of the frame only have to be narrow to fit into the well. After all, wells are often drilled on the surface of the earth to study the subsoil, and it is a sin not to use new and old wells.

First, the reduced surface impedance is measured δ equation (5). In this case, a frame is used, which is usually included in the complex of MSI equipment. Next, a similar frame is made, but having other dimensions to fit freely in the well. Calibration of the new frame is made by measuring the known reduced surface impedance. Next, a new frame and an ungrounded insulated electrical

wire are lowered in the form of a probe to a depth of the well. A new frame measures the horizontal component of the magnetic field H_φ, and vertical electric wire vertical component of electric field E_z. Component является горизонтальной, и ортогональной осям *r* и *z*. Reduced surface impedance δ can be called tangential, since it is located along the horizontal components of the magnetic field H_φ and electric field E_r, and is calculated according to the formula known to us equation (5):

$$\delta = -\frac{1}{\mu_{0m} c}\frac{E_{r0}}{H_{\varphi 0}}\Big|_{z=0}. \quad (27)$$

In here μ_{0m} is magnetic constant, and *c* is the speed of light.

Measured impedance by value of the component of the electromagnetic field in the well (horizontal magnetic field H_φ and vertical electric field E_z), can be called normal impedance δ^n. It is calculated by the formula

$$\delta^n = -\frac{1}{\mu_{0m} c}\frac{E_z}{H_\varphi}, \quad (28)$$

and turns out to be equal

$$\delta^n = \frac{k_0^{\,2}}{k^2}\sqrt{1-\delta^2} = \frac{\delta^2}{\sqrt{1-\delta^2}}. \quad (29)$$

Hence, in particular, neglecting the square of the impedance in the square root, we come to the formula (22). Here is the wave number in the atmosphere $k_0 = \omega / c$, and the square of the wave number in the terrestrial media.

$$k^2 = \frac{\omega^2}{c^2}\left(\varepsilon + \frac{i\sigma}{\varepsilon_0 \omega}\right). \quad (30)$$

In here ε and σ - the desired dielectric constant and electrical conductivity of the earth's rock at depth. Normal impedance, as shown by the result (29), does not depend on the vertical coordinate. If the medium is homogeneous, then regardless of the depth of the probe's descent into the well, the normal impedance will always be the same. However, the real terrestrial environment is heterogeneous, so the normal impedance measured at different depths of the probe will be different. This circumstance will make it possible to judge the properties of rocks lying in the depths of the lithosphere, in particular the presence of minerals.

When the normal impedance is known from the measurements, it is now easy to reconstruct the dielectric constant values from the result equation (29):

$$\varepsilon = \mathrm{Re}\frac{\sqrt{1-\delta^2}}{\delta^n}, \quad (31)$$

and electrical conductivity:

$$\sigma = \varepsilon_0 \omega\, \mathrm{Im}\,\frac{\sqrt{1-\delta^2}}{\delta^n}. \quad (32)$$

In here Re is valid part, Im is imaginary part.

If the meanings are known for a priori reasons ε and σ, and with them the square of the wave number (30), then the given surface impedance can be found from the relation (resulting from expression (29)).

$$\delta = \frac{k_0}{k}\sqrt{\frac{1}{2}\left(\sqrt{1+\left(\frac{2k}{k_0}\right)^2}-1\right)}. \quad (33)$$

Task. Try to find out whether from such measurements it is possible to establish the magnetic permeability of the earth's interior.

Hint. Start with Maxwell's equations containing magnetic permeability.

8. How the Electromagnetic Field Penetrates into the Impedance Medium

Two methods can be used to calculate the components of an electromagnetic field. The first is to construct a wave equation with a source for the vector potential. For the latter, the solution is expressed as the Sommerfeld integral, from where all the components of the fields are further located in article [12]. The second simpler method is to construct a wave equation for the single non-zero component of the magnetic field H_φ. This method was carried out by solving the wave equation by the method of separating variables in article [13]. For the convenience of references, we present the results of calculations for non-zero components of the electromagnetic field in a continuous medium, expressed through the given surface impedance (*K* is a constant that does not play a role in determining the impedance):

$$H_\varphi = -ik_0\sqrt{1-\delta^2}\frac{K}{\sqrt{r}}exp\left(-i\omega t + ik_0 r\sqrt{1-\delta^2} - ik_0\frac{1-\delta^2}{\delta}z\right). \quad (34)$$

$$E_r = i\omega\delta\sqrt{1-\delta^2}\frac{K}{\sqrt{r}}exp\left(-i\omega t + ik_0 r\sqrt{1-\delta^2} - ik_0\frac{1-\delta^2}{\delta}z\right). \quad (35)$$

$$E_z = i\omega\delta^2\frac{K}{\sqrt{r}}exp\left(-i\omega t + ik_0 r\sqrt{1-\delta^2} - ik_0\frac{1-\delta^2}{\delta}z\right). \quad (36)$$

Now, according to (5), we find that the magnitude δ is just the superficial impedance given. And from the formula (5) follows the result formula (4). Evaluation of the established fields shows that in free space and in the dielectric layer pattern, electric fields do not change, although in a dielectric electric fields are less than them in free space in $\frac{1}{\varepsilon_1}$, where is ε_1 is dielectric constant of dielectric medium.

In the conductive base, the electric field has basically

only a horizontal component: if taken $E_{z0}=1$, that $E_{z1}=\frac{1}{\varepsilon_1}$ and $E_{z2}=\delta^2$. The reduction of the electric field in the dielectric layer is consistent with the general concept of introducing a dielectric constant. Further $E_{r0}=\delta$, $E_{r1}=\frac{\delta}{\varepsilon_1}$ и $E_{r2}=\delta$.

For an ideal conductor, its resistivity tends to zero. Along with it, impedance will tend to zero. Then from the obtained estimates it follows that in the conductor the longitudinal and vertical components of the electric field, together with the impedance, rush to zero. Together with them, the entire vector of the electric field will be zero, as required by the determination of the conductive material - the electric field does not penetrate into the conductor in book [14]. We now know how an electric field does not penetrate a conductor.

The magnitude of magnetic induction in all media has not changed much; if $B_{y0}=1$ then and $B_{y1}=1$, $B_{y2}=1$. Qualitatively, the picture for the electric field is shown in Figure 5.

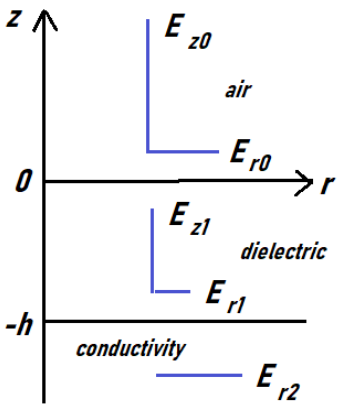

Figure 5. Horizontal and vertical components of the electric field (in relative units).

9. Conclusions

The paper introduces the basic concept and magnitude when measuring the electromagnetic field near the earth's surface - impedance. It is shown how the antennas of the IPI device are oriented, and how the coordinate system is set. It is established why the phase difference of the electromagnetic field component is limited to the limits from zero to minus ninety degrees. The introduction of the basic electrophysical characteristics of a continuous medium - dielectric constant and electrical conductivity - is considered. For a homogeneous medium, the dependence of impedance on electrophysical quantities is given. The Riccati equation for impedance is given. Not only the horizontal arrangement of the electrical cable is considered, but also the vertical one. The latter allows you to explore the electrical parameters of the media.

Funding

Work done in Laboratory Electromagnetic Diagnostics Institute of Physical Materials Science of the Siberian Branch RAS on the state budget project "Development of the fundamental foundations of diffusion HF-VHF and UHF radio waves in inhomogeneous impedance channels".

Conflict of Interest

There is no conflict of interest.

References

[1] Balkhanov, V.K., Bashkuev, Yu.B., 2022. Electromagnetic surface impedance, geoelectric homogeneous, two-layer and gradient media, Sommerfeld integral, 2nd ed.

[2] Parfentyev, P.A., Pertel, M.I., 1991. Device for measuring surface impedance in the SDV-SV band in the Earth-Ionosphere waveguide, Gylym, 133, Alma-Ata.

[3] Feinberg, E.L., 1999. Propagation of radio waves along the earth's surface. Fizmatlit, Moscow.

[4] Berdnik, S.L., Penkin, D.Yu., Katrich, V.A., et al., 2014. The use of the concept of surface impedance in electrodynamic problems (75 years later). Radiophysics and Radio Astronomy. 19(1), 57-80.

[5] Miller, M.A., Talanov, V.I., 1961. The use of the concept of surface impedance in the theory of surface electromagnetic waves. Izvestiya vuzov, Sir. Radiophysics. 4(5).

[6] Shchukin, A.N., 1940. Propagation of radio waves. Military-Maritime, Moscow; Leningrad, Publishing House.

[7] Balkhanov, V.K., Bashkuev, Yu.B., Angarkhaeva, L.Kh., 2017. New Horizons in Mathematical Physics. 1(3).
DOI: https://dx.doi.org/10.22606/nhmp.2017.13002

[8] Balkhanov, V.K., Bashkuev, Yu.B., Angarkhaeva, L.Kh., 2018. Surface Impedance of a Highly Inductive Two-layer Medium. Technical Physics. 63(3), 438-442.
DOI: https://doi.org/10.1134/S1063784218030015

[9] Markov, G.T., Chaplin, A.F., 1983. Excitation of electromagnetic waves. Radio & Communications, Moscow.

[10] Balkhanov, V.K., Advokatov, V.R., Bashkuev, Yu.B., 2014. Deformation of a fresh-water ice cover due to

the capillary oscillations of underlying water. Technical Physics. 59(8), 1255-1256.
DOI: https://doi.org/10.1134/S1063784214080040

[11] Fock, V.A., 1933. Theory of Determining the Resistance of Rocks by the Method of Logging. Moscow-Leningrad, GTTI.

[12] Balkhanov V.K., Bashkuev, Yu.B., Angarkhaeva, L.Kh., 2019. Vector Potential of Electromagnetic Wave above Strongly Inductive Two-Layer Earth Surface. Technical Physics September. 64(9), 1361-1366.
DOI: https://doi.org/10.1134/S1063784219 090032

[13] Balkhanov, V.K., Advocates, V.R., Bashkuev, Yu.B., 2014. Averaged electrical characteristics of the "forest layer" and the height of the forest cover. Technical Physics. 84(8), 132-135.
DOI: https://doi.org/10.1134/S1063784214080039

[14] Landau, L.D., Lifshitz, E.M., Pitaevskii, L.P., 1984. Electrodynamics of Continuous Media. 8. (2nd ed. Butterworth-Heinemann).

BILINGUAL PUBLISHING CO.
Pioneer of Global Academics Since 1984

Non-Metallic Material Science
https://ojs.bilpublishing.com/index.php/nmms

REVIEW

Recent Progress in Superhydrophobic Coatings Using Molecular Dynamics Simulations and Experimental Techniques

Sushanta K. Sethi*

Department of Metallurgical Engineering & Materials Science, IIT Bombay, Powai, Mumbai, India

ARTICLE INFO

Article history
Received: 2 June 2022
Accepted: 20 June 2022
Published Online: 24 June 2022

Keywords:
Superhydrophobic surfaces
Self-clean coatings
Molecular dynamics (MD) simulations
Bio-mimetic superhydrophobic surfaces
Chemical vapor deposition
Anti-corrosion coatings

ABSTRACT

Superhydrophobic (SH) coatings are intended to resist a surface from corrosion and thereby increases the product life duration. It is also a promising solution to save cleaning costs and time by providing self-clean nature to the surface. This review article provides the most recent updates in designing SH surfaces and their characterizations adopted both in experimental and computational techniques. To gain a comprehensive perspective, the SH surfaces present in nature those are inspiring human beings to mimic such surfaces are introduced at the beginning of this article. Subsequently, different fabrication techniques undertaken recently to design artificial SH surfaces are briefly discussed. Recent progress in computations employed in the development of SH surfaces is then discussed. Next, the limitations in SH surfaces are addressed. Finally, perceptiveness of different strategies and their limitations are presented in the concluding remarks and outlook. Overall, this mini review article brings together and highlights the significant advancements in fabrication of superhydrophobic surfaces which may surely help the early-stage researchers/scientists to plan their work accordingly.

1. Introduction

Superhydrophobic (SH) surfaces in nature demonstrating water contact angle (WCA) > 150° have enticed substantial topical research attention owing to their potential applications in many industrial sectors [1-4]. Fundamentally, this SH nature is a physicochemical phenomenon, wherein the physical appearance (surface texture) of a surface in combination with its chemical nature (low surface energy) combinedly helps to enhance the phobic nature of repelling water [1,5]. Before fabricating any artificial SH surface, it is better to first understand the self-clean surfaces present in nature. Lotus leaf [4,6,7], rice leaf [8,9], taro leaf [10,11], butterfly wings [12-14], water-strider legs [15], rose petals [16-18], and gecko feet [19-21] are the most exemplary cases present in nature exhibiting SH characteristics. Barthlott *et al.* [7] have investigated the self-clean nature of lotus leaf and found that there is a presence of (nano-scaled) epicuticular waxes superimposed over (micro-scaled) epidermal cells

*Corresponding Author:
Sushanta K. Sethi,
Department of Metallurgical Engineering & Materials Science, IIT Bombay, Powai, Mumbai, India;
Email: ssethi@pe.iitr.ac.in; sksethi@iitb.ac.in

DOI: https://doi.org/10.30564/nmms.v4i1.4768

combinedly provide a dual scale surface to surface. Both these textures are hydrophobic in nature and hence enable the surface to provide sufficient repellence nature against water. When water drops fall on the lotus leaf surface, it forms a completely spherical shape which can easily be rolled down the surface taking the dirt particles along with it. Likewise, the rice leaf surface is consisted of micro papillae that is superimposed by epicuticular waxy nano bumps and in butterfly wings the presence of hierarchical scales with micro grooves. Such surfaces demonstrate SH characteristics simultaneously providing drag reduction with several fluids. Basically this super hydrophobicity is governed by two prime factors as described earlier by Wenzel [22] and Cassie Baxter [23]. The intrinsic hydrophobic material presents at the extreme surface and the micro and nano-scale roughness on the topography. Scientists and researchers have utilized several techniques to fabricated biomimetic SH surfaces. The details of the various approaches are summarized in the subsequent section.

2. Fabrications Techniques

This section addresses the most used fabrication techniques for SH surfaces. Techniques such as spraying [24,25], chemical etching [26-28], lithography [29,30], electrospinning [31,32], surface wrinkling [33,34], chemical vapor deposition (CVD) [35-37], layer-by-layer coating [38,39], and photolithography laser surface treatment [40,41] are the numerous approaches for reported in recent years.

Spray coating is one of the most used techniques which is carried out by using a spray gun. A micron-level thickness with/without multi-layer coatings can be easily done in this technique. Zhang *et al.* [42] have fabricated a robust fluorine-free SH surface with a self-clean effect by first coating epoxy resin on a surface and then spraying silica nanoparticles and dodecyltrimethoxysilane to induce roughness and thereby reduce the surface energy. The coated surface demonstrated a water contact angle of >153°, which also can be used for oil-water separation applications. In the same line, Polizos *et al.* [43] reported a scalable technique for developing anti-soiling coatings based on SH surfaces by using the spray coating method. The authors have used polymer binders and silica nanoparticles and obtained a WCA of > 166°. Hence, this unique fabrication technique is a promising technique for producing SH surfaces for outdoor and indoor applications.

Chemical etching is another approach to designing SH surfaces; wherein etchant chemicals are used to produce corrugated surfaces. Varshney *et al.* [44] have prepared SH brass surfaces using a two-step process. In the first step, they have used a chemical etching method with a mixture of hydrochloric and nitric acids and then treatment with lauric acid. With the help of this etching technique, they obtained an adequate rough surface that demonstrated a WCA of > 173°. The authors also proposed its wide application in self-cleaning and anti-fogging applications.

Lithography is a non-complicated and dynamic approach that was developed to prepare different grades of nano/micro-structured surfaces over large areas. Jinpeng *et al.* [45] have used an ultrafast laser to develop nano/micro hierarchical structures on a metal surface with tunable micro-cones. Such a SH surface can withstand 70 abrasion cycles, 28 minutes of solid particles impact, or 500 peeling tape cycles and still can show a WCA of > 150°. This article explains the promising possibility of accomplishing excellent durability for real-time applications. Feng *et al.* [46] have reported a novel, versatile and efficient method for the fabrication of microscopic hierarchical SH surfaces with the presence of both micro and nano-scale textures using the electron-beam lithography technique.

SH coatings can also be prepared by using the electrospinning process. Radwan *et al.* [47] successfully fabricated PVDF/ZnO-based SH coating using this technique, which demonstrates a contact angle of 155° and contact angle hysteresis (CAH) of 4.5°. Though there were a number of literature reporting different coating techniques to design PVDF/ZnO based SH coating with excellent phobic nature but the significance of the study reported by Radwan and co-workers [47] are: (i) the authors have used a very low ZnO concentration without compromising with its phobic nature, (ii) an excellent dispersion was attained without any usage of dispersing agent, (iii) the ZnO filler doesn't phase out with time, (iv) the entire fabrication is a one-step process and (v) the formulated coating material demonstrates excellent corrosion protection nature.

Surface wrinkling is a spontaneous process of generating a rough surface. Scientists use this mechanism to fabricate corrugated surface-based SH surfaces. This phenomenon occurs due to the mismatch in elasticity among the underneath shrinkable substrate and the top rigid coated layer. Upon allowing the substrate to shrink, the first waves appear in the top layer and as more stress is applied, they turn into wrinkles and finally into folds [48-51]. Using this approach, Scarratt *et al.* [52] reported the fabrication of both single scale and hierarchical SH surfaces prepared by exploiting the spontaneous wrinkling of rigid Teflon film on two types of shrinkable plastic substrates. The hierarchical wrinkled SH surface exhibits an excellent WCA of ~172° with a very low CAH of 2°. The authors suggested that such an approach can be tuned to obtain micro-to-nano scale wrinkled surfaces in one step.

Chemical vapor deposition (CVD) is another versatile approach to preparing a SH surface by reducing the surface free energy. Rezaei *et al.* [53] have prepared a bio-inspired SH coating by using vinyltrimethoxysilane and triethyl orthosilicate as surface-modifying molecules and ammonia. This material showed a WCA of >160° and a low sliding angle of <5°. The major advantages of this article were, (i) the authors have explored an all gas-phase and simultaneous deposition and modification of silane coating to avoid HCl production and post-treatment of silica nanoparticles. With the help of ammonia, they were able to lower the working temperature, which suggests that such technology can also be used for temperature-sensitive materials. There are several types of CVD processes, such as atmospheric pressure chemical vapor deposition (APCVD), aerosol-assisted chemical vapor deposition (AACVD), and plasma enhanced chemical vapor deposition (PECVD), used for fabricating SH surfaces. A comprehensive study can be found elsewhere [54]. The fundamental behind such different approaches to developing SH surfaces are like to reduce the surface free energy either by using low surface energy treatment or by designing corrugated surfaces.

2.1 Treatment with Low Surface Energy Polymers

Irrespective of the substrate used, the surface energy treatment relies on silane and fluorine chemistry. The silane treatment is generally preferred over fluorine treatment considering the toxicity impact on the environment. Researchers employ poly(vinylidene fluoride) (PVDF) [55,56], per(fluoro octane) (PFO) [57,58], fluoroalkyl silane (FAS-17) [59-61], and poly (tetrafluoroethylene) (PTFE) [62] etc., for fluoro treatment while making the desired surface SH. For silane treatment researchers use (tridecafluoro-1,1,2,2-tetrahydrooctyl)-1-trichlorosilane [63], tetraethyl orthosilicate (TEOS) [64-66] and heptadecafluoro-1,1,2,2-tetrahydrodecyltriethoxysilane [67].

2.2 Designing of Hierarchical Surface Texture

Besides low surface energy treatment, the construction of micro or nanoscale rough surfaces is also an important technique to reduce the water attachment to the surface [1]. Achieving a WCA of > 120° is not feasible only by surface treatment with low-energy polymers. Hence, combining low surface energy with surface roughness is obligatory to obtain a SH surface with an excellent WCA of >150° and a very low CAH of <5°. There are several ways to prepare micro/nano-scaled rough surfaces with enhanced contact angles, a few of them have already been discussed earlier in the manuscript in section 2. It can be considered that keeping the material same if the contact angle on a flat surface is around 100°-120°. Then it can be turned into 150°-160° only by adding roughness to it [68]. Two different models have been developed earlier to explain this effect, as depicted in Figure 2. When the rough pillars allow sufficient water molecules to impregnate the grooves, then a maximum wetting condition can be obtained, which is known as the Wenzel model [69]. When the rough pillars prevent the water molecules from entering inside it, thusly the water remains in a completely spherical shape and sits above the pillars then; it is considered as Cassie-Baxter model [23]. In this case the rolling angle is also very low.

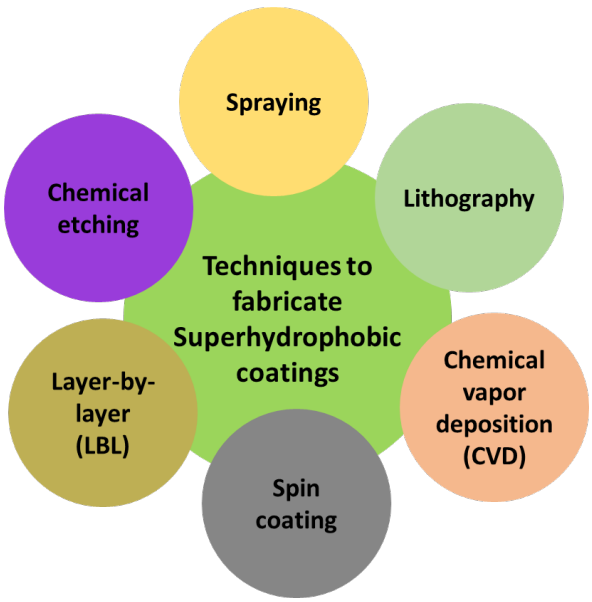

Figure 1. Various fabrication techniques used for SH coating materials.

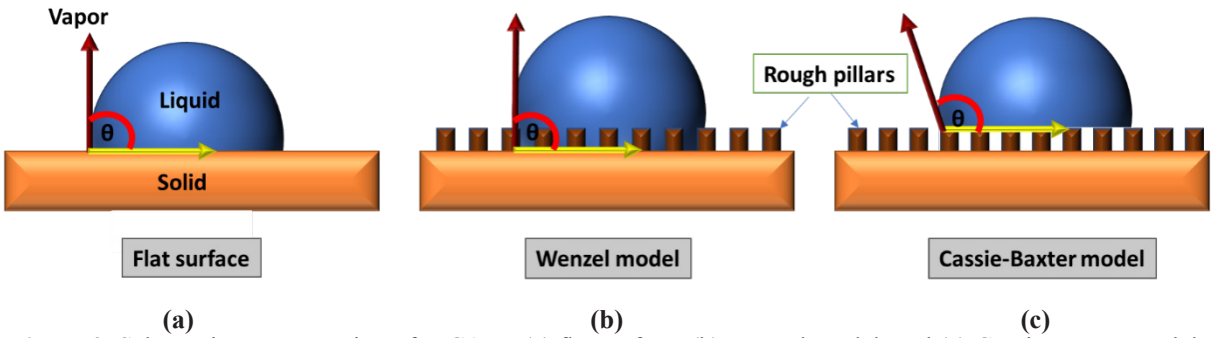

Figure 2. Schematic representation of WCA on (a) flat surface, (b) Wenzel model, and (c) Cassie-Baxter model.

3. Application of Molecular Dynamics (MD) Simulation in SH Coatings

MD simulations have long been served as a fundamental tool to gain understanding in different sectors of research, such as estimation of interaction energy among various polymers/fillers [70-73], the surface energy of polymers/metals [74], interfacial shear strength [75], and wetting characteristics [76], etc. computational scientists use different water models such as SPCE, SPC, TIP3P, and TIP4P [77], etc. to replicate the water droplets in MD simulations and then predict the SH nature of the desired surface [76]. To predict the simulated contact angle a number of methods have been developed, like microscopic wetting phenomena [78], float method [79], and quick-hull recursive method [80], etc. The details of each computational technique can be found elsewhere [76].

In this line, Sethi *et al.* [81] have first predicted the blend compatibility among poly(dimethylsiloxane) (PDMS) and poly(vinyl acetate) (PVAc) using MD simulations. Later on, the authors have predicted the easy-clean behavior of the PVAc-PDMS blend [82] and obtained a contact angle of 97 ± 1° for a 20:80 ratio of PVAc to PDMS. Owing to the incompatibility among polar PVAc and nonpolar PDMS, the authors have then grafted PVAc over PDMS, considering the same 20:80 concentration of PVAc to PDMS [83]. Subsequently, they have incorporated CNT [84] and ZnO QDs [74] in PVAc-g-PDMS and computed the WCAs, and found 109±2° (4 wt.% of ZnO QDs) and 117±2° (3 wt.% of CNT). In another work, Sethi *et al.* [85] have computed the impact of roughness on wettability. They have modelled different surfaces with varying grooves and studied how it affects the surface wettability. In the same line, Xu *et al.* [86] have investigated the variation in wetting characteristics with varying defect % in graphene oxide. They found that the WCA increased from 70° to 82°, when the defective concentration increased from 0 to 10% (as shown in Figure 3). Similarly, researchers have computed the SH nature of graphene [86,87], poly(vinylidene fluoride) (PVDF) [55], poly(ethylene terephthalate) (PET) [88] and sphalerite [89], etc. using MD simulations.

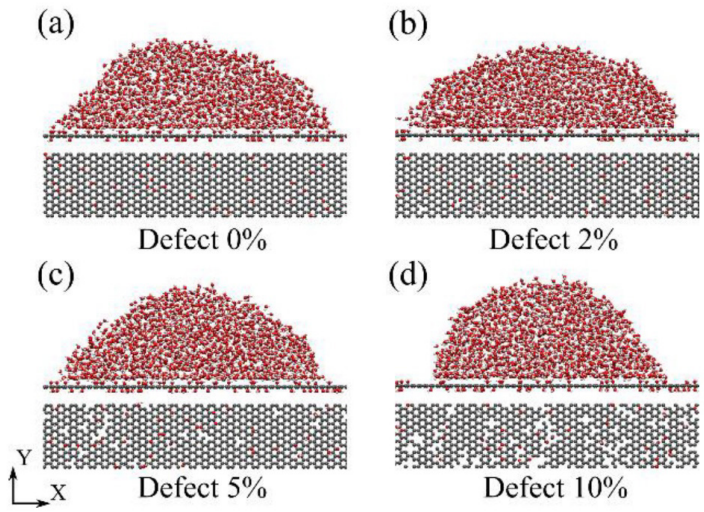

Figure 3. Illustration of water contact angle profile of graphene oxide with varying defect %. (a) 0%, (b) 2%, (c) 5%, and (d) 10% defects in graphene oxide. Reprinted with permission from [86].

4. Limitations to the Development of SH Coatings

Although there is a wide range of applications for SH surfaces, still not many commercial products have been developed with these functionalities. Some of the major limitations have been listed and discussed below.

4.1 Cost of Materials

A few of the fabrication techniques discussed above are very costly. Sometimes the fabrication process may also require costly materials. Techniques such as lithography and templates cannot be used on very large areas. Hence, designing small part surfaces and stitching them together to make a larger one may sometimes also increase the overall product's cost [29,30,46].

4.2 Technique to Fabricate SH Material

Out of all possible techniques, a few of them have limitations to their usage. Like template technique cannot be used for all materials, the attainable geometry is also limited [90].

4.3 Durability of Coating Material

Any SH surface requires either a dual-scale or nano-scale roughness. Most of the time, such roughness is not durable enough to withstand the abrasion caused during their daily usage; thereby, it losses its SH nature [91]. Especially in the case of polymers, it is not very easy to maintain the corrugated textured surface for a long duration. Also, there is a standoff among its SH nature and its durability, as it is not very easy to bond any SH nanoparticle without degrading or affecting its SH nature [92].

4.4 Precipitation/Condensation Issue

Since the SH surfaces are designed to repel water hence at below certain dew points when water condenses, it may not get repelled by the developed surface. Hence the surface can substantially be wetted when the temperature of the environment changes [93,94].

4.5 Health and Environmental Effects

The most developed SH surfaces are derived from fluoro-based polymers. Though a little concentration may not have that much impact on health or the environment but a higher concentration may cause serious health issues during product manufacturing, usage, or disposal. It may cause fever, teeth and bone decay, harm to kidney nerves and muscles, and eye and nose irritations [95,96]. Besides, most of the silanes are poisonous.

5. Summary and Conclusions

In this review article, the latest achievements in the field of SH surface generation have been presented. The basic idea to create a SH surface is by surface treatment with low surface energy and construction of a rough-textured surface to enhance the water repellence nature. Properties like self-cleaning, anti-corrosion, and anti-sticking have been identified for such SH surfaces and have a broad potential application. Here, several fabrication techniques alongside computational techniques to gain some fundamental insight into wetting behavior were reviewed and discussed. Several manufacturing processes have certain limitations; those are also briefly discussed. Limitations such as cost, technique, durability, and environmental impact are of great challenge for researchers. Designing fluorine-free eco-friendly self-clean coating materials are receiving overwhelming attention owing to its non-health hazardous effect. The importance of industrial SH surfaces requires enhanced durability, for which scientists have developed robust self-clean surfaces with highly stable and durable surface characteristics. Simultaneously, the durable SH surfaces may be merged with some additional functionalities to develop multi-functional surfaces/coating materials that can be further strengthened to be developed in future work in this field.

Author Contributions

Sushanta K. Sethi: Writing, reviewing, editing, and conceptualization.

Conflict of Interest

The author declares there is no conflict of interest.

References

[1] Sethi, S.K., Manik, G., 2018. Recent Progress in Super Hydrophobic/Hydrophilic Self-Cleaning Surfaces for Various Industrial Applications: A Review. Polymer Plastics Technology & Engineering. 57, 1932-1952.
DOI: https://doi.org/10.1080/03602559.2018.1447128

[2] Sethi, S.K., Gogoi, R., Manik, G., 2021. Plastics in Self-Cleaning Applications. Reference Module in Materials Science and Materials Engineering.
DOI: https://doi.org/10.1016/B978-0-12-820352-1.00113-9

[3] Si, Y., Guo, Z., 2015. Superhydrophobic nanocoatings: from materials to fabrications and to applications. Nanoscale. 7, 5922-5946.
DOI: https://doi.org/10.1039/C4NR07554D

[4] Bhushan, B., Jung, Y.C., 2011. Natural and biomi-

metic artificial surfaces for superhydrophobicity, self-cleaning, low adhesion, and drag reduction. Progress in Materials Science. 56, 1-108.
DOI: https://doi.org/10.1016/j.pmatsci.2010.04.003

[5] Vinogradova, O.I., Dubov, A.L., 2012. Superhydrophobic textures for microfluidics. Mendeleev Communications. 22, 229-236.
DOI: https://doi.org/10.1016/j.mencom.2012.09.001

[6] Wang, F., Li, S., Wang, L., 2017. Fabrication of artificial super-hydrophobic lotus-leaf-like bamboo surfaces through soft lithography. Colloids & Surfaces A Physicochemical & Engineering Aspects. 513, 389-395.
DOI: https://doi.org/10.1016/j.colsurfa.2016.11.001

[7] Barthlott, W., Neinhuis, C., 1997. Purity of the sacred lotus, or escape from contamination in biological surfaces. Planta. 202, 1-8.
DOI: https://doi.org/10.1007/s004250050096

[8] Bixler, G.D., Bhushan, B., 2013. Fluid drag reduction and efficient self-cleaning with rice leaf and butterfly wing bioinspired surfaces. Nanoscale. 5, 7685-7710.
DOI: https://doi.org/10.1039/C3NR01710A

[9] Liu, M., Wang, S., Jiang, L., 2017. Nature-inspired superwettability systems. Nature Reviews Materials. 27(2), 1-17.
DOI: https://doi.org/10.1038/natrevmats.2017.36

[10] Chen, Y.P., Wang, H.W., Yao, Q.F., et al., 2017. Biomimetic taro leaf-like films decorated on wood surfaces using soft lithography for superparamagnetic and superhydrophobic performance. Journal of Materials Science. 52, 7428-7438.
DOI: https://doi.org/10.1007/s10853-017-0976-y

[11] Huang, J.A., Zhang, Y.L., Zhao, Y.Q., et al., 2016. Superhydrophobic SERS chip based on a Ag coated natural taro-leaf. Nanoscale. 8, 11487-11493.
DOI: https://doi.org/10.1039/C6NR03285K

[12] Bixler, G.D., Theiss, A., Bhushan, B., et al., 2014. Anti-fouling properties of microstructured surfaces bio-inspired by rice leaves and butterfly wings. Journal of Colloid and Interface Science. 419, 114-133.
DOI: https://doi.org/10.1016/j.jcis.2013.12.019

[13] Han, Z., Fu, J., Wang, Z., et al., 2017. Long-term durability of superhydrophobic properties of butterfly wing scales after continuous contact with water. Colloids & Surfaces A Physicochemical & Engineering Aspects. 518, 139-144.
DOI: https://doi.org/10.1016/j.colsurfa.2017.01.030

[14] Bixler, G.D., Bhushan, B., 2012. Bioinspired rice leaf and butterfly wing surface structures combining shark skin and lotus effects. Soft Matter. 8, 11271-11284.
DOI: https://doi.org/10.1039/C2SM26655E

[15] Gao, X., Jiang, L., 2004. Water-repellent legs of water striders. Nature. 4327013(432), 36.
DOI: https://doi.org/10.1038/432036a

[16] Bhushan, B., Her, E.K., 2010. Fabrication of superhydrophobic surfaces with high and low adhesion inspired from rose petal. Langmuir. 26, 8207-8217.
DOI: https://doi.org/10.1021/la904585j

[17] Bhushan, B., Nosonovsky, M., 2010. The rose petal effect and the modes of superhydrophobicity. Philosophical Transactions of the Royal Society A: Mathematical, Physical and Engineering Sciences. 368, 4713-4728.
DOI: https://doi.org/10.1098/rsta.2010.0203

[18] Shao, Y., Zhao, J., Fan, Y., et al., 2020. Shape memory superhydrophobic surface with switchable transition between "Lotus Effect" to "Rose Petal Effect". Chemical Engineering Journal. 382, 122989.
DOI: https://doi.org/10.1016/j.cej.2019.122989

[19] Liu, K., Du, J., Wu, J., et al., 2012. Superhydrophobic gecko feet with high adhesive forces towards water and their bio-inspired materials. Nanoscale. 4, 768-772.
DOI: https://doi.org/10.1039/C1NR11369K

[20] Autumn, K., Liang, Y.A., Hsieh, S.T., et al., 2000. Adhesive force of a single gecko foot-hair. Nature. 405, 681-685.
DOI: https://doi.org/10.1038/35015073

[21] Sethi, S.K., Manik, G., Sahoo, S.K., 2019. Fundamentals of superhydrophobic surfaces. in Superhydrophobic Polymer Coatings. 3-29. Elsevier.
DOI: https://doi.org/10.1016/B978-0-12-816671-0.00001-1

[22] Wenzel, R.N., 1936. Resistance of Solid Surfaces to wetting by water. Industrial and Engineering Chemistry. 28, 988-994.
DOI: https://doi.org/10.1021/ie50320a024

[23] Cassie, A.B.D., Baxter, S., 1944. Wettability of porous surfaces. Transactions of the Faraday Society. 40, 546.
DOI: https://doi.org/10.1039/TF9444000546

[24] Li, Y., Chen, Sh.Sh., Wu, M.Ch., et al., 2014. All Spraying Processes for the Fabrication of Robust, Self-Healing, Superhydrophobic Coatings. Advanced Materials. 26, 3344-3348.
DOI: https://doi.org/10.1002/adma.201306136

[25] Cai, C.J., Teng, S.C., Guo, J., et al., 2016. Superhydrophobic surface fabricated by spraying hydrophobic R974 nanoparticles and the drag reduction in water. Surface & Coatings Technology. 307, 366-373.
DOI: https://doi.org/10.1016/j.surfcoat.2016.09.009

[26] Huang, Y., Sarkar, D.K., Grant Chen, X., 2015. Su-

perhydrophobic aluminum alloy surfaces prepared by chemical etching process and their corrosion resistance properties. Applied Surface Science. 356, 1012-1024.
DOI: https://doi.org/10.1016/j.apsusc.2015.08.166

[27] Qian, B., Shen, Z., 2005. Fabrication of superhydrophobic surfaces by dislocation-selective chemical etching on aluminum, copper, and zinc substrates. Langmuir. 21, 9007-9009.
DOI: https://doi.org/10.1021/la051308c

[28] Han, M., Go, S., Ahn, Y., 2012. Fabrication of Superhydrophobic Surface on Magnesium Substrate by Chemical Etching. Bulletin- Korean Chemical Society. 33, 1363-1366.
DOI: https://doi.org/10.5012/bkcs.2012.33.4.1363

[29] Shiu, J.Y., Kuo, C.W., Chen, P., et al., 2004. Fabrication of Tunable Superhydrophobic Surfaces by Nanosphere Lithography. Chemistry of Materials. 16, 561-564.
DOI: https://doi.org/10.1021/cm034696h

[30] Pozzato, A., Zilio, S.D., Fois, G., et al., 2006. Superhydrophobic surfaces fabricated by nanoimprint lithography. Microelectronic Engineering. 83, 884-888.
DOI: https://doi.org/10.1016/j.mee.2006.01.012

[31] Zhou, Z. & Wu, X. F., 2015. Electrospinning superhydrophobic-superoleophilic fibrous PVDF membranes for high-efficiency water-oil separation. Materials Letters. 160, 423-427.
DOI: https://doi.org/10.1016/j.matlet.2015.08.003

[32] Zhu, M., Zuo, W., Yu, H., et al., 2006. Superhydrophobic surface directly created by electrospinning based on hydrophilic material. Journal of Materials Science. 4112(41), 3793-3797.
DOI: https://doi.org/10.1007/s10853-005-5910-z

[33] Chen, T.L., Huang, Ch.Y., Xie, Y.T., et al., 2019. Bioinspired Durable Superhydrophobic Surface from a Hierarchically Wrinkled Nanoporous Polymer. Acs Applied Materials & Interfaces. 11, 40875-40885.
DOI: https://doi.org/10.1021/acsami.9b14325

[34] Li, Y., Dai, S., John, J., et al., 2013. Superhydrophobic surfaces from hierarchically structured wrinkled polymers. Acs Applied Materials & Interfaces. 5, 11066-11073.
DOI: https://doi.org/10.1021/am403209r

[35] Ma, M.L., Mao, Y., Gupta, M., et al., 2005. Superhydrophobic Fabrics Produced by Electrospinning and Chemical Vapor Deposition.
DOI: https://doi.org/10.1021/MA0511189

[36] Sun, W., Wang, L., Yang, Z., et al., 2017. Fabrication of polydimethylsiloxane-derived superhydrophobic surface on aluminium via chemical vapour deposition technique for corrosion protection. Corrosion Science. 128, 176-185.
DOI: https://doi.org/10.1016/j.corsci.2017.09.005

[37] Şimşek, B., Karaman, M., 2020. Initiated chemical vapor deposition of poly(hexafluorobutyl acrylate) thin films for superhydrophobic surface modification of nanostructured textile surfaces. Journal of Coatings Technology and Research. 17, 381-391.
DOI: https://doi.org/10.1007/s11998-019-00282-7

[38] Li, Y., Liu, F., Sun, J.A., 2009. Facile layer-by-layer deposition process for the fabrication of highly transparent superhydrophobic coatings. Chemical Communications. 0, 2730.
DOI: https://doi.org/10.1039/B900804G

[39] Lopez-Torres, D., Elosua, C., Hernaez, M., et al., 2015. From superhydrophilic to superhydrophobic surfaces by means of polymeric Layer-by-Layer films. Applied Surface Science. 351, 1081-1086.
DOI: https://doi.org/10.1016/j.apsusc.2015.06.004

[40] Gwon, T.M., Kim, J.H., Choi, G.J., et al., 2016. Mechanical interlocking to improve metal-polymer adhesion in polymer-based neural electrodes and its impact on device reliability. Journal of Materials Science. 51, 6897-6912.
DOI: https://doi.org/10.1007/s10853-016-9977-5

[41] Lee, S.H., Lee, J.H., Park, Ch.W., et al., 2014. Continuous fabrication of bio-inspired water collecting surface via roll-type photolithography. International Journal of Precision Engineering and Manufacturing-Green Technology. 12(1), 119-124.
DOI: https://doi.org/10.1007/s40684-014-0016-1

[42] Zhang, Z.H., Wang, H.J., Liang, Y.H., et al., 2018. One-step fabrication of robust superhydrophobic and superoleophilic surfaces with self-cleaning and oil/water separation function. Scientific Reports. 81(8), 1-12.
DOI: https://doi.org/10.1038/s41598-018-22241-9

[43] Polizos, G., Jang, G.G., Smith, D.B., et al., 2018. Transparent superhydrophobic surfaces using a spray coating process. Solar Energy Materials and Solar Cells. 176, 405-410.
DOI: https://doi.org/10.1016/j.solmat.2017.10.029

[44] Varshney, P., Mohapatra, S.S., 2018. Durable and regenerable superhydrophobic coatings for brass surfaces with excellent self-cleaning and anti-fogging properties prepared by immersion technique. Tribology International. 123, 17-25.
DOI: https://doi.org/10.1016/j.triboint.2018.02.036

[45] Han, J., Cai, M., Lin, Y., et al., 2018. Comprehensively durable superhydrophobic metallic hierarchi-

cal surfaces Via tunable micro-cone design to protect functional nanostructures. Rsc Advances. 8, 6733-6744.
DOI: https://doi.org/10.1039/C7RA13496G

[46] Feng, J., Tuominen, M.T., Rothstein, J.P., 2011. Hierarchical Superhydrophobic Surfaces Fabricated by Dual-Scale Electron-Beam-Lithography with Well-Ordered Secondary Nanostructures. Advanced Functional Materials. 21, 3715-3722.
DOI: https://doi.org/10.1002/adfm.201100665

[47] Radwan, A.B., Mohamed, A.M.A., Abdullah, A.M., et al., 2016. Corrosion protection of electrospun PVDF-ZnO superhydrophobic coating. Surface & Coatings Technology. 289, 136-143.
DOI: https://doi.org/10.1016/j.surfcoat.2015.12.087

[48] Fu, C.C., Grimes, A., Long, M., et al., 2009. Tunable Nanowrinkles on Shape Memory Polymer Sheets. Advanced Materials. 21, 4472-4476.
DOI: https://doi.org/10.1002/adma.200902294

[49] Genzer, J., Groenewold, J., 2006. Soft matter with hard skin: From skin wrinkles to templating and material characterization. Soft Matter. 2, 310-323.
DOI: https://doi.org/10.1039/B516741H

[50] Manna, U., Carter, M.C.D., Lynn, D.M., 2013. "Shrink-to-Fit" Superhydrophobicity: Thermally-Induced Microscale Wrinkling of Thin Hydrophobic Multilayers Fabricated on Flexible Shrink-Wrap Substrates. Advanced Materials. 25, 3085-3089.
DOI: https://doi.org/10.1002/adma.201300341

[51] Huntington, M.D., Engel, C.J., Hryn, A.J., et al., 2013. Polymer nanowrinkles with continuously tunable wavelengths. ACS Applied Materials & Interfaces. 5, 6438-6442.
DOI: https://doi.org/10.1021/am402166d

[52] Scarratt, L.R.J., Hoatson, B.S., Wood, E.S., et al., 2016. Durable Superhydrophobic Surfaces via Spontaneous Wrinkling of Teflon AF. ACS Applied Materials & Interfaces. 8, 6743-6750.
DOI: https://doi.org/10.1021/acsami.5b12165

[53] Rezaei, S., Manoucheri, I., Moradian, R., et al., 2014. One-step chemical vapor deposition and modification of silica nanoparticles at the lowest possible temperature and superhydrophobic surface fabrication. Chemical Engineering Journal. 252, 11-16.
DOI: https://doi.org/10.1016/j.cej.2014.04.100

[54] Xu, S., Wang, Q., Wang, N., 2021. Chemical Fabrication Strategies for Achieving Bioinspired Superhydrophobic Surfaces with Micro and Nanostructures: A Review. Advanced Engineering Materials. 23, 2001083.
DOI: https://doi.org/10.1002/adem.202001083

[55] Kitabata, M., Taddese, T., Okazaki, S., 2018. Molecular Dynamics Study on Wettability of Poly(vinylidene fluoride) Crystalline 8and Amorphous Surfaces. Langmuir. 34, 12214-12223.
DOI: https://doi.org/10.1021/acs.langmuir.8b02286

[56] Wang, F.J., Li, C.Q., Tan, Z.S., et al., 2013. PVDF surfaces with stable superhydrophobicity. Surface & Coatings Technology. 222, 55-61.
DOI: https://doi.org/10.1016/j.surfcoat.2013.02.004

[57] Kumar, N., Manik, G., 2016. Molecular dynamics simulations of polyvinyl acetate-perfluorooctane based anti-stain coatings. Polymer (Guildf). 100, 194-205.
DOI: https://doi.org/10.1016/j.polymer.2016.08.019

[58] Cui, Z., Wang, Q., Xiao, Y., et al., 2008. The stability of superhydrophobic surfaces tested by high speed current scouring. Applied Surface Science. 254, 2911-2916.
DOI: https://doi.org/10.1016/j.apsusc.2007.09.062

[59] Saleema, N., Sarkar, D.K., Gallant, D., et al., 2011. Chemical nature of superhydrophobic aluminum alloy surfaces produced via a one-step process using fluoroalkyl-silane in a base medium. ACS Applied Materials & Interfaces. 3, 4775-4781.
DOI: https://doi.org/10.1021/am201277x

[60] Wang, Y., Liu, X., Zhang, H., et al., 2015. Superhydrophobic surfaces created by a one-step solution-immersion process and their drag-reduction effect on water. Rsc Advances. 5, 18909-18914.
DOI: https://doi.org/10.1039/C5RA00941C

[61] Liu, H., Chen, T., Yang, H., et al., 2016. Biomimetic fabrication of robust self-assembly superhydrophobic surfaces with corrosion resistance properties on stainless steel substrate. Rsc Advances. 6, 43937-43949.
DOI: https://doi.org/10.1039/C6RA06500G

[62] Chen, W., Fadeev, A.Y., Hsieh, M.C., et al., 1999. Ultrahydrophobic and Ultralyophobic Surfaces: Some Comments and Examples.
DOI: https://doi.org/10.1021/LA990074S

[63] Zhai, L., Cebeci, F.C., Cohen, R.E., et al., 2004. Stable superhydrophobic coatings from polyelectrolyte multilayers. Nano Letters. 4, 1349-1353.
DOI: https://doi.org/10.1021/nl049463j

[64] Xue, C.H., Jia, S.T., Zhang, J., et al., 2008. Preparation of superhydrophobic surfaces on cotton textiles. Science & Technology of Advanced Materials. 9, 35008.
DOI: https://doi.org/10.1088/1468-6996/9/3/035008

[65] Peng, P.P., Ke, Q., Zhou, G., et al., 2013. Fabrication of microcavity-array superhydrophobic surfaces using an improved template method. Journal of Colloid

and Interface Science. 395, 326-328.
DOI: https://doi.org/10.1016/j.jcis.2012.12.036

[66] Rahmawan, Y., Xu, L., Yang, S., 2013. Self-assembly of nanostructures towards transparent, superhydrophobic surfaces. Journal of Materials Chemistry A. 1, 2955-2969.
DOI: https://doi.org/10.1039/C2TA00288D

[67] Ge, D., Yang, L., Zhang, Y., et al., 2014. Transparent and superamphiphobic surfaces from one-step spray coating of stringed silica nanoparticle/sol solutions. Particle & Particle Systems Characterization. 31, 763-770.
DOI: https://doi.org/10.1002/ppsc.201300382

[68] Yang, C., Tartaglino, U., Persson, B.N.J., 2006. Influence of surface roughness on superhydrophobicity. Physical Review Letters. 97, 1-4.
DOI: https://doi.org/10.1103/PhysRevLett.97.116103

[69] Wenzel, R.N., 1936. Resistance of solid surfaces to wetting by water. Industrial & Engineering Chemistry. 28, 988-994.
DOI: https://doi.org/10.1021/ie50320a024

[70] Agrawal, G., Samal, S.K., Sethi, S.K., et al., 2019. Microgel/silica hybrid colloids: Bioinspired synthesis and controlled release application. Polymer (Guildf). 178, 121599.
DOI: https://doi.org/10.1016/j.polymer.2019.121599

[71] Maurya, A.K., Gogoi, R., Sethi, S.K., et al., 2021. A combined theoretical and experimental investigation of the valorization of mechanical and thermal properties of the fly ash-reinforced polypropylene hybrid composites. Journal of Materials Science. 56, 16976-16998.
DOI: https://doi.org/10.1007/s10853-021-06383-2

[72] Shankar, U., Sethi, S.K., Singh, B.P., et al., 2021. Optically transparent and lightweight nanocomposite substrate of poly(methyl methacrylate-co-acrylonitrile)/MWCNT for optoelectronic applications: an experimental and theoretical insight. Journal of Materials Science. 5630(56), 17040-17061.
DOI: https://doi.org/10.1007/s10853-021-06390-3

[73] Saini, A., Yadav, C., Sethi, S.K., et al., 2021. Microdesigned Nanocellulose-Based Flexible Antibacterial Aerogel Architectures Impregnated with Bioactive Cinnamomum cassia. ACS Applied Materials & Interfaces. 13, 4874-4885.
DOI: https://doi.org/10.1021/acsami.0c20258

[74] Sethi, S.K. et al., 2020. Fabrication and Analysis of ZnO Quantum Dots Based Easy Clean Coating: A Combined Theoretical and Experimental Investigation. ChemistrySelect. 5, 8942-8950.
DOI: https://doi.org/10.1002/slct.202001092

[75] Gogoi, R., Sethi, S.K., Manik, G., 2021. Surface functionalization and CNT coating induced improved interfacial interactions of carbon fiber with polypropylene matrix: A molecular dynamics study. Applied Surface Science. 539.
DOI: https://doi.org/10.1016/j.apsusc.2020.148162

[76] Sethi, S.K., Kadian, S., Manik, G., 2022. A Review of Recent Progress in Molecular Dynamics and Coarse-Grain Simulations Assisted Understanding of Wettability. Archives of Computational Methods in Engineering. 1, 1-27.
DOI: https://doi.org/10.1007/s11831-021-09689-1

[77] Zielkiewicz, J., 2005. Structural properties of water: Comparison of the SPC, SPCE, TIP4P, and TIP5P models of water. The Journal of Chemical Physics. 123, 104501.
DOI: https://doi.org/10.1063/1.2018637

[78] Hautman, J., Klein, M.L., 1991. Microscopic wetting phenomena. Physical Review Letters. 67, 1763-1766.
DOI: https://doi.org/10.1103/PhysRevLett.67.1763

[79] Malani, A., Raghavanpillai, A., Wysong, E.B., et al., 2012. Can dynamic contact angle be measured using molecular modeling? Physical Review Letters. 109, 1-5.
DOI: https://doi.org/10.1103/PhysRevLett.109.184501

[80] Khalkhali, M., Kazemi, N., Zhang, H., et al., 2017. Wetting at the nanoscale: A molecular dynamics study. Journal of Chemical Physics. 146.
DOI: https://doi.org/10.1063/1.4978497

[81] Sethi, S.K., Soni, L., Manik, G., 2018. Component compatibility study of poly(dimethyl siloxane) with poly(vinyl acetate) of varying hydrolysis content: An atomistic and mesoscale simulation approach. Journal of Molecular Liquids. 272, 73-83.
DOI: https://doi.org/10.1016/j.molliq.2018.09.048

[82] Sethi, S.K., Soni, L., Shankar, U., et al., 2020. A molecular dynamics simulation study to investigate poly(vinyl acetate)-poly(dimethyl siloxane) based easy-clean coating: An insight into the surface behavior and substrate interaction. Journal of Molecular Structure. 1202, 127342.
DOI: https://doi.org/10.1016/j.molstruc.2019.127342

[83] Sethi, S.K., Shankar, U., Manik, G., 2019. Fabrication and characterization of non-fluoro based transparent easy-clean coating formulations optimized from molecular dynamics simulation. Progress in Organic Coatings. 136.
DOI: https://doi.org/10.1016/j.porgcoat.2019.105306

[84] Sethi, S.K., Manik, G., 2021. A combined theoretical and experimental investigation on the wettability of MWCNT filled PVAc-g-PDMS easy-clean coating.

Progress in Organic Coatings. 151, 106092.
DOI: https://doi.org/10.1016/j.porgcoat.2020.106092

[85] Sethi, S.K., Singh, M., Manik, G., 2020. A multi-scale modeling and simulation study to investigate the effect of roughness of a surface on its self-cleaning performance. Molecular Systems Design & Engineering.
DOI: https://doi.org/10.1039/D0ME00068J

[86] Xu, K., Zhang, J.Ch., Hao, X.L., et al., 2018. Wetting properties of defective graphene oxide: A molecular simulation study. Molecules. 23, 1-8.
DOI: https://doi.org/10.3390/molecules23061439

[87] Huang, C., Xu, F., Sun, Y., 2017. Effects of morphology, tension and vibration on wettability of graphene: A molecular dynamics study. Computational Materials Science. 139, 216-224.
DOI: https://doi.org/10.1016/j.commatsci.2017.07.017

[88] Zimmermann, J., Reifler, F.A., Fortunato, G., et al., 2008. A simple, one-step approach to durable and robust superhydrophobic textiles. Advanced Functional Materials. 18, 3662-3669.
DOI: https://doi.org/10.1002/adfm.200800755

[89] Mohseni, M., Abdollahy, M., Poursalehi, R., et al., 2018. Quantifying the spreading factor to compare the wetting properties of minerals at molecular level - case study : sphalerite surface. 54, 646-656.
DOI: https://doi.org/10.5277/ppmp1856

[90] Li, X.M., Reinhoudt, D., Crego-Calama, M., 2007. What do we need for a superhydrophobic surface? A review on the recent progress in the preparation of superhydrophobic surfaces. Chemical Society Reviews. 36, 1350.
DOI: https://doi.org/10.1039/B602486F

[91] Bhushan, B., Jung, Y.C., 2011. Natural and biomimetic artificial surfaces for superhydrophobicity, self-cleaning, low adhesion, and drag reduction. Progress in Materials Science. 56, 1-108.
DOI: https://doi.org/10.1016/j.pmatsci.2010.04.003

[92] Aegerter, M.A., Almeida, R., Soutar, A., et al., 2008. Coatings made by sol-gel and chemical nanotechnology. Journal of SOL-GEL Science and Technology. 472(47), 203-236.
DOI: https://doi.org/10.1007/s10971-008-1761-9

[93] Miljkovic, N., Enright, R., Wang, E.N., 2013. Modeling and optimization of superhydrophobic condensation. Journal of Heat Transfer. 135.
DOI: https://doi.org/10.1115/1.4024597

[94] Boreyko, J.B., Chen, C.H., 2009. Self-propelled dropwise condensate on superhydrophobic surfaces. Physical Review Letters. 103, 184501.
DOI: https://doi.org/10.1103/PhysRevLett.103.184501

[95] Sananda, D., Biplab, G., 2016. Fluoride Fact on Human Health and Health Problems: A Review. Medical & Clinical Reviews. 2.
DOI: https://doi.org/10.21767/2471-299X.1000011

[96] Wang, W., Lockwood, K., Boyd, L.M., et al., 2016. Superhydrophobic Coatings with Edible Biowaxes for Reducing or Eliminating Liquid Residues of Foods and Drinks in Containers. ACS Applied Materials & Interfaces. 8, 18664-18668.
DOI: https://doi.org/10.1021/acsami.6b06958

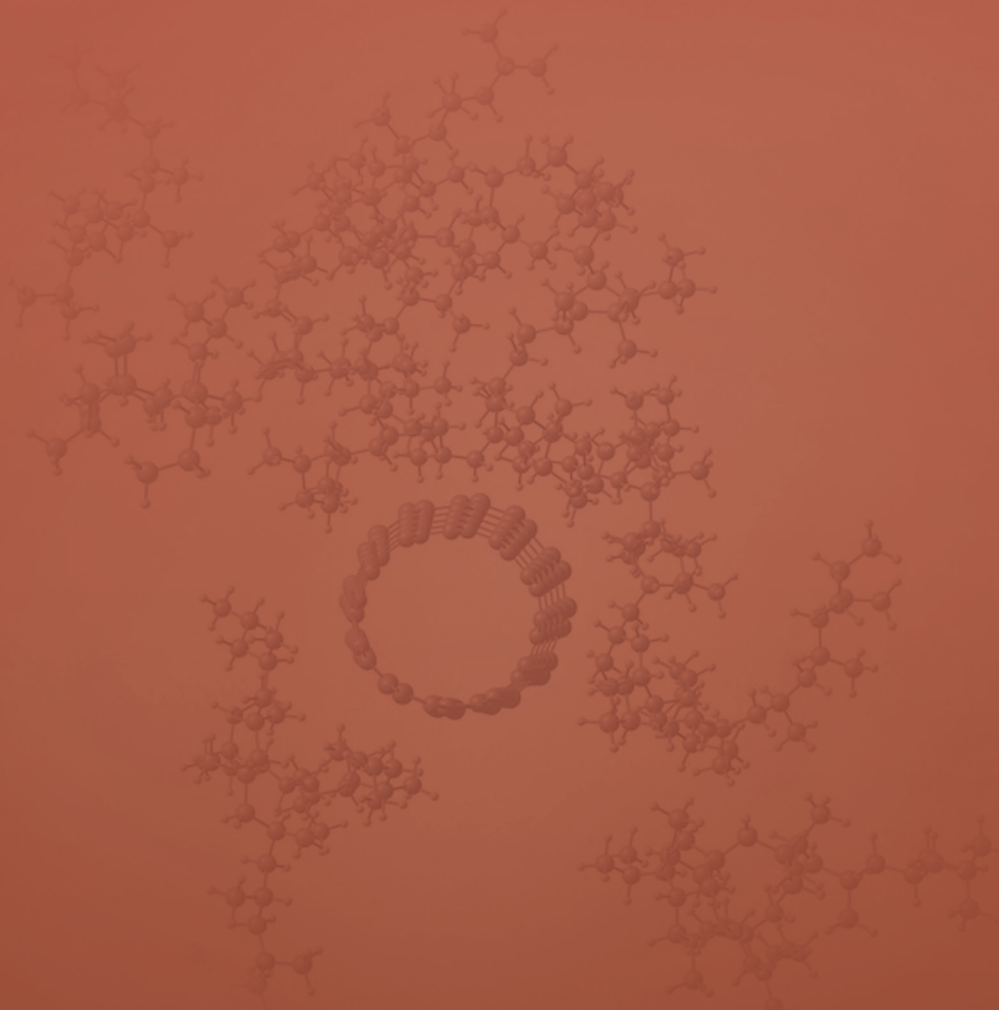

BILINGUAL
PUBLISHING CO.
Pioneer of Global Academics Since 1984

Tel:+65 65881289
E-mail: contact@bilpublishing.com
Website:ojs.bilpublishing.com

2661-3301
01
9 772661 330222